NASA CONTRACTOR REPORT

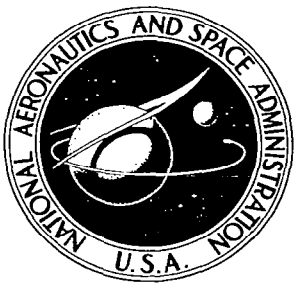

NASA CR-61

NASA CR-680

STUDY OF ELECTROLYTIC DISSOCIATION OF CO_2-H_2O USING A SOLID OXIDE ELECTROLYTE

by J. Weissbart and W. H. Smart

Prepared by
LOCKHEED MISSILES & SPACE COMPANY
Palo Alto, Calif.
for Ames Research Center

NATIONAL AERONAUTICS AND SPACE ADMINISTRATION • WASHINGTON, D. C. • FEBRUARY 1967

NASA CR-680

STUDY OF ELECTROLYTIC DISSOCIATION OF CO_2-H_2O USING A SOLID OXIDE ELECTROLYTE

By J. Weissbart and W. H. Smart

Prepared under Contract No. NAS 2-2810 by
LOCKHEED MISSILES & SPACE COMPANY
Palo Alto, Calif.

for Ames Research Center

NATIONAL AERONAUTICS AND SPACE ADMINISTRATION

For sale by the Clearinghouse for Federal Scientific and Technical Information
Springfield, Virginia 22151 – Price $2.50

FOREWORD

The research reported here was performed at the Lockheed Palo Alto Research Laboratory, Palo Alto, California, from 6 May 1965 to 6 May 1966, under Contract No. NAS 2-2810. The work was done by Dr. J. Weissbart, who was the project leader, Dr. W. H. Smart, and Mr. L. S. Rowley. Dr. T. Wydeven, Environmental Control Research Branch, NASA Ames Research Center, Moffett Field, California, was the technical monitor.

ABSTRACT

Samples of the system $(ZrO_2)_{0.85-x}(CeO_2)_x(CaO)_{0.15}$ in the range $x = 0$ to $x = 0.45$ were prepared from solution and sintered at 1600° C in oxygen. Analysis by x-ray diffraction indicates that a single-phase solid solution having the fluorite structure is formed. Replacement of Zr^{+4} by the large Ce^{+4} ions produces a linear increase of the lattice parameter from 5.133Å (0 mole % CeO_2) to 5.285Å (45 mole % CeO_2). A comparison of densities measured pycnometrically with those calculated from the lattice parameters indicates that the oxygen ion vacancy concentration remains constant.

AC conductivity measurements were carried out at 400−1200° C and oxygen partial pressures of 1 atm (oxygen) to approximately 10^{-30} atm (CO/CO_2 mixtures). From plots of conductivity versus temperature (log σ vs. 1/T) an activation energy of 1.14 eV was found for oxygen ion mobility in the 0−45 mole % ceria range corroborating the constancy of the oxygen ion vacancy concentration.

Below $P_{O_2} \sim 10^{-3}$ atm, an electronic component is present due to the reduction of Ce^{+4} to Ce^{+3} in contrast to zirconia-calcia in the absence of ceria. In this pressure range each curve of log σ vs. 1/T at constant CO/CO_2 ratio consists of two approximately linear sections showing a transition from predominately ionic (high T) to predominately electronic (low T) conductivity. The transition temperature is a function of the mole % ceria and CO/CO_2 ratio. The temperature coefficient for electronic conductivity decreases asymptotically with increasing mole % ceria approaching an approximately constant value of 0.5 eV at 15 to 30 mole % ceria. Conductivity versus P_{O_2} isotherms show a constant value of conductivity in the high pressure region, an increase to a conductivity maximum and then a decrease in σ with decreasing P_{O_2} in the low pressure region.

The degree of reduction of Ce^{+4} to Ce^{+3} and the increase in oxygen vacancy concentration was measured as a function of T and total ceria by a microweighing technique. A linear relationship exists between n in CeO_n and P_{O_2}. For reduced samples (to 20.4 mole % Ce^{+3}) the fluorite type structure is retained and the lattice parameter as a function of mole fraction of Ce^{+4} and Ce^{+3} found to be

$$a_o(\text{Å}) = 5.134 + 0.00338\,[Ce^{+4}] + 0.00223\,[Ce^{+3}]$$

For solid solutions containing $Ce^{+3} \leq 0.2$ (mole fraction) a disorder equilibrium exists between $Ce^{+4} - Ce^{+3}$ ions and oxygen ions, vacancies, and P_{O_2}. A value of -133 kcal/mole O_2 was found for the partial molar enthalpy of reaction at $CeO_{1.83}$. An equation was derived describing the experimental curves.

A tentative explanation for the appearance of electronic conductivity follows. In the removal of oxygen from the lattice, electrons are trapped on Ce^{+4} sites forming Ce^{+3}. Electronic conduction occurs by a hopping mechanism between Ce^{+3} and Ce^{+4} while Zr^{+4} and Ca^{+2} are blocking to electron transfer. For a constant value of ceria, a constant number of continuous paths for possible electron transfer exist through the structure. Electronic σ is proportional to the Ce^{+3} ion concentration and to an exponential term containing an activation energy term. At 770° C and 15 mole % ceria, an approximately linear increase in electronic σ with increase of Ce^{+3} from 0 to 2 mole % takes place. From 2 to 4 mole % the electronic conductivity is approximately constant and with further increase of Ce^{+3} the σ decreases. This decrease in conductivity is tentatively ascribed to an increase in the oxygen vacancy concentration leading to a large drop in the ionic conductivity component.

Electrolysis of CO_2-H_2O was carried out in a 15 mole % calcia-zirconia tube cell at temperatures less than 800° C. The CO_2 flow rate was varied between 5 and 15 ml/min and current densities of 50, 100 and 150 mA/cm^2 for a 1 cm^2 electrode area were used. Runs were made in the absence of water and with additions of from 0.2 to 2.4 ml/min of water vapor to the CO_2 stream. The beneficial catalytic influence

of water vapor was demonstrated by an increase of oxygen current efficiency from 19% (no water) to 100% at 785° C and 50 mA/cm^2 and from 15% (no water) to 76% at 790° C and 100 mA/cm^2. Because only small additions of water are required, a calculation of the water shift equilibrium at 730–793° C shows that essentially only reduction of CO_2 should take place.

Cells were also constructed by the use of sealed oxide disks. Electrolysis using 0 and 3 mole % ceria disk cells indicate that loss in current efficiency resulting from the component of electronic conductivity in 3 mole % ceria is compensated by the lower voltage required.

Electrolysis of 6.5, 10 and 15 mole % ceria disks did not give reproducible values of oxygen current efficiencies due to a variable back-flow of oxygen. The reasons for these anomalous results are being investigated. The construction of a one-eighth man laboratory model CO_2 electrolyzer is discussed.

CONTENTS

ILLUSTRATIONS

TABLES

Section 1
INTRODUCTION

An important problem in maintaining a closed ecological environment in a manned space vehicle is the removal of respiratory carbon dioxide and the regeneration of its oxygen content.

Several different approaches for the regeneration of oxygen from carbon dioxide are under investigation in various laboratories. A method for the removal of CO_2 and regeneration of O_2 that has many attractive features is that of electrolysis in a solid oxide electrolyte cell. In addition, electrolysis of H_2O and CO_2-H_2O may also be carried out in the same cell.

Serious disadvantages of present solid oxide electrolyte cells are the high operating temperatures of around 1000°C needed to obtain 100% current efficiency and low electrolyte resistance. Some of the problems of high temperature operation are increased power consumption to maintain the operating temperature, increased weight and volume due to insulation required, high temperature cell construction and operation problems and problems of reliability. It is, therefore, of importance for the ultimate success of this method to be able to lower the operating temperature significantly below 1000°C.

Several approaches in the synthesis of oxygen ion conducting electrolytes and in the electrolysis procedures may profitably be investigated in order to attain the goal of high energy efficiencies at relatively low operating temperatures.

This program consists of a study of the electrochemical properties of oxygen ion solid electrolytes having the imperfect fluorite structure. These studies are being made in the temperature range 500 – 1000°C. The aim is to be able to operate cells made from these electrolytes for the electrolytic dissociation of CO_2-H_2O at temperatures

below 1000°C, preferably in the region 600 – 750°C at high energy efficiencies. In order to accomplish this objective, 100 percent oxygen ion conductors as well as several conductors with compositionally built-in variable amounts of an electronic component have been synthesized. In order to be able to optimize the electrolyte electrochemical parameters for the required cell operating conditions, both types of electrolytes were studied with respect to a number of important physical-chemical factors.

There has been much progress in recent years in various applications of oxygen ion solid conductors based on the investigations of the physical-chemical, structural, and electrochemical properties of mixed oxide solid solutions. The criteria for electrolytes with optimum properties are well understood, especially for open-circuit measurements. This is true as well for open-circuit diffusion-migration phenomena, a-c conductivity dependence on O_2 partial pressure, the Nernst-Einstein relation between electrical conductivity of an ionic species, and its self-diffusion coefficient, etc. However, studies on the absolute specific conductance versus composition and temperature, and those carried out on galvanic and electrolytic cells with current flow through the oxygen ion conducting electrolytes, have resulted in many contradictory data and differing interpretations of the various phenomena observed. These problems may be at least in part due to such factors as: impurities present in the oxide materials, poorly-characterized and irreproducible experimental conditions (especially gas phase compositions and current-voltage conditions – particularly electrode potentials), insufficient attention paid to time-dependent effects and their cause or causes, and difficulties associated with the theoretical interpretation of cell polarization effects complicated by the presence of a variable electronic component in the electrolyte.

Interest in the use of solid oxide cells for the exchange of chemical and electrical energy predates the turn of the century. Nernst (Ref. 1) first showed qualitatively that oxygen can be transferred electrolytically in a $(ZrO_2)_{0.85}(Y_2O_3)_{0.15}$ electrolyte, since known as Nernstmasse or Nernst glower. Quantitative measurements of oxygen transferred versus current passed were made on Nernst glower material by Weininger and Zemany (Ref. 2) who obtained 7–80% current efficiency depending on many factors in their experimental conditions. The validity of Faraday's law to within 1% for

solid oxide conductors was first shown by Weissbart and Ruka (Ref. 3) for the composition $(ZrO_2)_{0.85}(CaO)_{0.15}$ near 1000 °C. Following a recommendation by Schottky (Ref. 4) for the use of solid oxygen ion conductors in fuel cells, Bauer and Preis (Ref. 5) constructed the first solid oxide electrolyte fuel cell using Nernst glower material. Small currents were obtained but according to the authors, cation conductivity damaged the cell, and this work was discontinued. Further work was carried out by Bauer and Preis (Ref. 5) on mixtures consisting of clay, cerium oxide, and tungsten trioxide "solid" electrolytes. These materials undergo irreversible changes during cell operation, and a reinvestigation of these materials by Broers (Ref. 6) showed that these electrolytes were molten salts held in a solid or semi-solid matrix. A high temperature fuel cell with $(ZrO_2)_{0.85}(CaO)_{0.15}$ using H_2 and carbonaceous fuel was investigated in the temperature range 800–1100 °C by Weissbart and Ruka (Ref. 7) and found to have a cell output limited essentially by the electrolyte resistance. This cell was reinvestigated by Binder et al. (Ref. 8) with essentially similar results. Activation polarization with gas mixtures consisting only of CO-CO_2 in oxide galvanic cells were observed at relatively high temperatures by Neuimin and co-workers (Ref. 9) and at LMSC (Ref. 10). On electrolysis of CO_2 or the reversal of the fuel cell reaction, Chandler and Oser (Ref. 11) found that the current efficiency was only 7.5 % at 750 °C with a ThO_2-La_2O_3 solid electrolyte. More recent work by Chandler (Ref. 12) has shown that 100 % current efficiency can be obtained at 1000 °C with ZrO_2-Y_2O_3 and other electrolytes but that the efficiency drops and is time dependent at lower operating temperatures.

Further improvement in our understanding of the physical and electrochemical characteristics of solid oxide electrolytes resulting from this research program holds the promise of developing a carbon dioxide reduction system having significant advantages over other techniques. The most important of these advantages are:

- The oxygen produced is pure
- The electrolyzer is invariant in operation
- No liquids are involved, hence no zero-gravity separation problem arises
- No electrolyte corrosion problems
- The CO produced may be used as an intermediate in food synthesis

Section 2

PREPARATION AND CHARACTERIZATION OF THE MIXED OXIDE SYSTEM $(ZrO_2)_{0.85-x}(CeO_2)_x(CaO)_{0.15}$

2.1 INTRODUCTION

The starting material of this ternary or pseudobinary oxide system is $(ZrO_2)_{0.85}(CaO)_{0.15}$. The mole % CaO is kept constant and the mole % CeO_2 is varied from zero to 45%. Although no information on this system is available in the literature, the ZrO_2-CaO oxide system with ZrO_2 as the host (solvent) oxide and CaO as the foreign (solute) oxide has been extensively studied in recent years. A host of information on the physical-chemical properties as well as the electrochemical is available in the literature. A recent excellent review of the literature of the ZrO_2-CaO and other oxide systems of interest as electrolyte materials is presented by Mobius (Ref. 13).

We are interested in ZrO_2-CaO solid solutions with the defect fluorite-type structure as electrolyte materials because of their relatively high electrical conductivity at high temperatures ascribed to the presence of oxygen ion vacancies in the anion sublattice. Zr^{+4} and Ca^{+2} ions are statistically distributed over the cation sites of the cation sublattice while anion vacancies are created in the anion sublattice to preserve electrical neutrality. The number of vacancies is equal to the number of molecules of solute CaO dissolved in the host oxide ZrO_2. This model, in contrast to the one where excess Ca^{++} ions occupy interstitial sites, was first experimentally substantiated by Hund (Ref. 14).

Considerable disagreement exists about the CaO composition limits of the cubic phase region of this system. Table 2-1 summarizes most of the available data.

Table 2-1

ZrO_2-CaO CUBIC PHASE REGION

Solution Range (mole % CaO)	Preparation (T °C)	Investigator
16–30	2000	Duwez et al. (Ref. 15)
10–20	1460	Hund (Ref. 14)
7–24	1800	Dietzel and Tobler (Ref. 16)
14–20	1400	
10–40	1500	Volchenkova and Palguev (Ref. 17)
12–22	1400	Tien and Subbarao (Ref. 18)

There is likewise considerable disagreement about electrical conductivity values for the same composition and temperature, e.g., $(ZrO_2)_{0.85}(CaO)_{0.15}$ at 1000 °C. This has been discussed recently by Tien and Subbarao (Ref. 18). Electronic conductivity makes only a negligible contribution to the total conduction according to Weissbart and Ruka (Ref. 3). These conclusions are valid only for the experimental conditions of open-circuit measurement, when current is drawn from a galvanic cell, or for electrolytic oxygen transfer. Under conditions where electrolysis of CO_2 proceeds, significant electronic conduction may be introduced and current efficiencies below 100% may result (Refs. 11, 12, and 19). These effects with $(ZrO_2)_{0.85-x}(CeO_2)_x(CaO)_{0.15}$ will be further discussed in other sections of this report.

There is also some disagreement in the literature about the existence of a conductivity maximum in the ZrO_2-CaO system. Trombe and Foex (Ref. 20) and Volchenkova and Palguev (Ref. 17) indicate a conductivity maximum at 15 mole % CaO, while Johansen and Cleary (Ref. 21) report a maximum at 12 mole % CaO. Tien and Subbarao (Ref. 18) conclude from their data that the conductivity decreases with increase of CaO content or anion vacancy concentration throughout the 13–20 mole % solid solution range which they found. For the reason that $(ZrO_2)_{0.85}(CaO)_{0.15}$ has a high oxygen ion conductivity, is near the conductivity maximum, and is a single phase material, it was chosen as the starting material in the ternary system under investigation.

Phase studies of solid solutions of the fluorite-type structure with CeO_2 as the host oxide in the binary system CeO_2-CaO with up to 15 mole % CaO have been made by Keler et al. (Ref. 22). Palguev and co-workers (Ref. 23) using an open-circuit cell EMF method have shown that for the ternary system $(Zr_{0.25}Ce_{0.75}O_2)_{1-x}(CaO)_x$ in reducing atmospheres appreciable electronic conductivity is introduced in the structure. The electrolyte disks become discolored due to formation of Ce_2O_3 and break apart. In general, binary or ternary systems with large amounts of CeO_2 as the host or predominant oxide are unstable in reducing atmospheres such as would be found at the CO_2 electrode.

Duwez and Odell (Ref. 24) have examined the binary zirconia-ceria oxide system. They found that the solubility gap is narrowed by the addition of a third component. At 2000°C complete solubility occurs on the addition of 13.8 mole % magnesium oxide to stabilize the zirconia. At lower temperatures the homogeneous phase decomposes again into a tetragonal and solid solution phase. At 1375°C the solubility gap extends approximately from 35 to 65 mole % ceria and at 1100°C the influence of MgO on the solubility completely disappears. At 1110°C, solid solution specimens containing 10 mole % ceria decompose into monoclinic zirconia and a tetragonal solid solution. These results may in large part be ascribed to the presence of the relatively small Mg^{+2} cation which leaves the cation sublattice and enters the interstitial positions of the fluorite-type structure.

It is therefore of interest to examine the $(ZrO_2)_{0.85-x}(CeO_2)_x(CaO)_{0.15}$ electrolyte system in order to determine that the solubility limits of the Ce^{+4} and Ce^{+3} oxides are not exceeded and that decomposition to two phases and the destruction of the electrolyte does not occur under the reducing conditions found at the CO/CO_2 electrode. The determination of the structure and phase relationship by x-ray and pycnometric density measurements on the mixed oxide system containing fully oxidized ceria, i.e., Ce^{+4}, is discussed below.

2.2 SPECIMEN PREPARATION

Chemically pure zirconium oxychloride and calcium carbonate, and cerium nitrate code 277 obtained from the Lindsay Division of the American Potash and Chemical

Corporation were used as the starting materials. Spectrographic analyses of these materials are given in Table 2-2. Duplicate samples of zirconium oxychloride and cerium nitrate were heated in air at 900°C to determine the oxide content.

Table 2-2

SPECTROCHEMICAL ANALYSIS OF STARTING MATERIALS

Elements Detected	Estimated Concentration (%)		
	$CaCO_3$	$Ce(NO_3)_3$	$ZrOCl_2$
Mg	0.03	0.07	0.002−0.007
Si		0.01	0.005
Ca		0.01	0.002−0.01
Ti			0.003
Mn	0.008		
Cu	<0.001		
Sr	0.03		
Ba	0.003		<0.01

An attempt was made to coprecipitate the Ca and Zr salts from solution as the hydroxides, after which the precipitate was filtered. The coprecipitate was then heated at 120°C, ground, heated at 1000°C, and pressed into discs which were then sintered for 10 hours at 1600°C. These discs turned out to be porous and this method was therefore abandoned.

The method employed to prepare the zirconia-calcia and zirconia-calcia-ceria specimens was that used by Kiukkola and Wagner (Ref. 25) for zirconia-calcia compositions with certain modifications. The salts were dissolved in the required proportions in concentrated nitric acid solution. The solution was evaporated to dryness in a porcelain dish and then heated overnight in an oven at 120°C. The powder was then ground in an agate mortar, heated overnight at 1000°C in a dense stabilized zirconia crucible and reground. The powder was pressed into disks 20 mm in diameter and 1/2 to 2 mm in thickness at a pressure of about 20,000 psi with no addition of binder. The specimens were placed on platinum or platinum-rhodium sheet inside a dense high purity

alumina tube and sintered in a flowing oxygen atmosphere at 1600°C for about 10 hr. The powders appeared homogeneous after firing at 1000°C with the zirconia-calcia powders being colored white while the powders containing ceria took on a yellowish tinge with increasing content of ceria. Disks sintered at 1600°C containing ceria appeared ivory white to yellow.

The disks were leak checked by placing them on a flat silicone rubber gasket resting on a Forsterite tube (American Lava Corporation). The disk holder is evacuated by means of a forepump and the pressure in the system is monitored by a Pirani gauge. Disks pumped down to approximately 20 microns (the lower limit of this pump system) and not penetrated by acetone sprayed on them were considered gas-tight. Porous disks could not be pumped down to this pressure and penetration of acetone would deflect the Pirani gauge meter. Only gas-tight disks were used for conductivity and cell measurements. The apparent density of disk specimens in comparison with the pycnometric density on powders is discussed below.

2.3 STRUCTURE AND PHASE RELATIONSHIP

Disk specimens sintered at 1600°C in oxygen were cooled in the furnace. The disks were ground to a fine powder in an agate mortar for x-ray examination to determine the phase or phases present and lattice parameters at ambient temperature. CuKα radiation with a nickel filter was used and Debye-Scherrer patterns were obtained on a GE XRD-5 x-ray diffractometer. Several samples were examined on a 57.3 mm Debye-Scherrer camera.

In the zirconia-calcia solid solution region, the lattice parameters increase linearly with increase of % CaO. Table 2-3 shows the lattice parameter values obtained for 15 and 20 mole % CaO and compares the change of lattice parameter $\Delta a_o/\Delta$ mole % CaO obtained from these two values with several literature values. The 15 mole % CaO lattice constants in the literature tend to cluster around 5.130–5.133 Å although several values 0.01 to 0.02 Å units lower are reported. Purity of the samples investigated and the sintering temperatures employed may account for this discrepancy.

Table 2-3

LATTICE PARAMETERS OF ZIRCONIA-CALCIA SOLID SOLUTIONS

Composition	a_o(Å)	Δa_o(Å)/Δ mole % CaO	Investigator
$(ZrO_2)_{0.85}(CaO)_{0.15}$	5.133	+0.0018	This work
$(ZrO_2)_{0.80}(CaO)_{0.20}$	5.142		
S.S. Phase Region		+0.0017	Tien and Subbarao (Ref. 18)
S.S. Phase Region		+0.0017	Dietzel and Tober (Ref. 16)
S.S. Phase Region		+0.0013	Hund (Ref. 14)

The lattice parameters obtained for specimens of composition $(ZrO_2)_{0.85-x}(CeO_2)_x(CaO)_{0.15}$ are presented in Table 2-4 and plotted in Fig. 2-1 (upper abscissa values).

Table 2-4

LATTICE PARAMETERS OF $(ZrO_2)_{0.85-x}(CeO_2)_x(CaO)_{0.15}$ SOLID SOLUTIONS

Composition (Mole % CeO_2)	Lattice Parameter a_o(Å)
0	5.133 ± 0.002
1.0	5.135
3.0	5.144
6.5	5.156
15.0	5.187
30.0	5.235
45.0	5.285

A single phase solid solution with fluorite-type structure was found in the whole composition range of CeO_2 investigated. The diffraction line values were extrapolated to obtain a_o according to the method of Nelson and Riley (Ref. 26). The variation of lattice constant with composition can be accounted for by the relative size or ionic radii of the ions, Ce^{+4} = 1.07 Å, Zr^{+4} = 0.93 Å (Ref. 13).

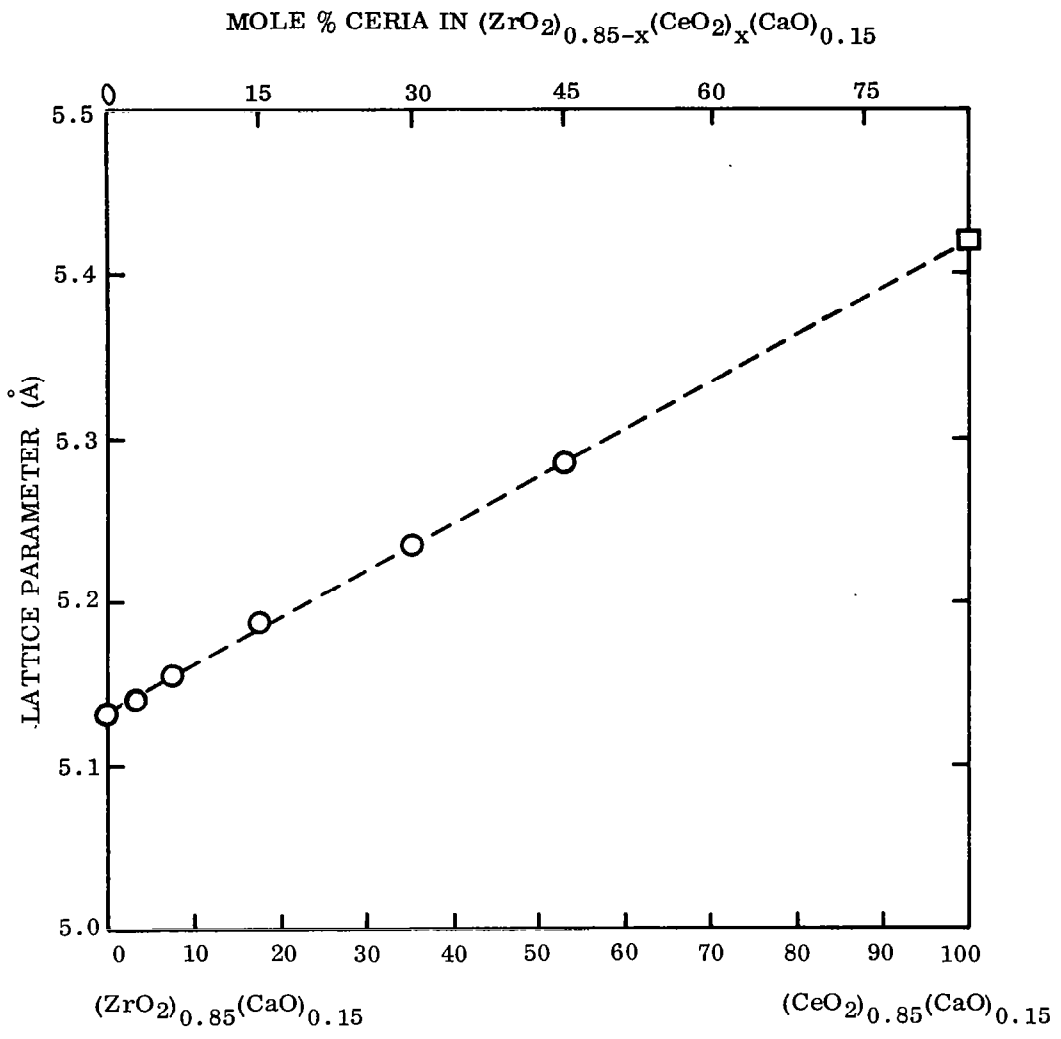

Fig. 2-1 Comparison of Lattice Parameters for the System $(ZrO_2)_{0.85-x}(CeO_2)_x(CaO)_{0.15}$

The lattice parameters were found to increase linearly from 5.133 Å for the solid solution with no CeO_2 to 5.285 Å for the 45 mole % CeO_2 solid solution. Electrolytes in this composition range kept at temperatures of 1000°C and lower for long periods of time should remain single phase materials with the fluorite-type structure in contrast to magnesia stabilized zirconia-ceria solutions which are unstable at these temperatures and decompose into two phases (Ref. 24).

A 30 mole % ceria sample used for electrical resistance measurements and held at temperatures between 1097 and 803°C for twenty-six days was subsequently examined by x-rays. Only lines of the one phase fluorite structure were present. The lattice parameter was found to be 5.230 ± 0.005 Å in good agreement with 5.235 ± 0.002 Å found with a similar sample heated to 1600°C and cooled to room temperature.

Keler and co-workers (Ref. 22) have reported a value of 5.420 Å for the solid solution $(CeO_2)_{0.85}(CaO)_{0.15}$ which also has a fluorite-type structure. Vegard's law holds that the lattice cell dimensions should vary linearly with concentration of solute added to the host solution. Assuming Vegard's law is obeyed on mixing $(ZrO_2)_{0.85}(CaO)_{0.15}$ and $(CeO_2)_{0.85}(CaO)_{0.15}$ we draw a straight line between the two a_o values as shown in Fig. 2-1. The lower and upper abscissa values are related to each other by the equation

$$(1 - y)\ [(ZrO_2)_{0.85}(CaO)_{0.15}] + y\,[(CeO_2)_{0.85}(CaO)_{0.15}] \rightarrow (ZrO_2)_{0.85-x}(CeO_2)_x(CaO)_{0.15} \qquad (2\text{-}1)$$

where $y = x/0.85$ and x and y are mole fractions. The experimentally determined a_o values for 3, 6.5, 15, 30, and 45 mole % ceria fall on the straight line agreeing in a satisfactory fashion with the interpolated a_o values.

The type of defect structure, e.g., vacancy or interstitial present in a mixed oxide crystal may be determined by comparison of the experimentally obtained pycnometric density with that calculated from lattice parameters.

The anion defect structure of zirconia-calcia solid solutions was first experimentally determined by Hund (Ref. 14) and confirmed by Rabenau (Ref. 27). When Zr^{+4} ions are replaced by Ce^{+4} ions in the cation sublattice, the anion defect structure should remain unaltered. For a constant value of 15 mole % CaO, the number of oxygen ion vacancies should remain constant at 15 mole %. For a completely filled cation sublattice consisting of 4 cations per unit cell in a fluorite-type structure the vacancy model density is

$$d_v = \frac{4[(0.85-x)\,ZrO_2 + x\,CeO_2 + 0.15\,CaO]}{NV} \qquad (2\text{-}2)$$

where $(0.85-x)\,ZrO_2$, $x\,CeO_2$, and $0.15\,CaO$ are the mole fractions of the molecular weights of these species, N is Avogadro's number, and $V\left(=a_o^3\right)$ is the unit cell volume obtained from the lattice parameters in Table 2-4. For comparison, assuming the anion sublattice of 8 oxygen ions per unit cell is complete and excess Ca^{++} ions occupy interstitial sites, the interstitial model density is

$$d_I = \frac{4.33[(0.85-x)\,ZrO_2 + x\,CeO_2 + 0.15\,CaO]}{NV} \qquad (2\text{-}3)$$

The calculated and measured densities are shown in Table 2-5 and Fig. 2-2. This oxide system therefore has a structure whose unit cell edge and density increase linearly with increasing mole % ceria while at the same time the number of oxygen vacancies remains constant. Additional vacancies are created by the reduction of Ce^{+4} to Ce^{+3} ions. Reduction of ceria is discussed in the section on Disorder Equilibrium.

The reported densities were measured on powders from disks sintered at 1600°C in oxygen for 10 hr, crushed and ground in an agate mortar.

The pycnometric fluid used was bicyclohexyl recommended by Ruby and Loveland (Ref. 28) for the determination of densities on fine powders. The bicyclohexyl used gave a density value of 0.8822 versus the literature value of 0.8825. All powder samples were first degassed, the fluid was added, and then further degassed. It was observed that disk

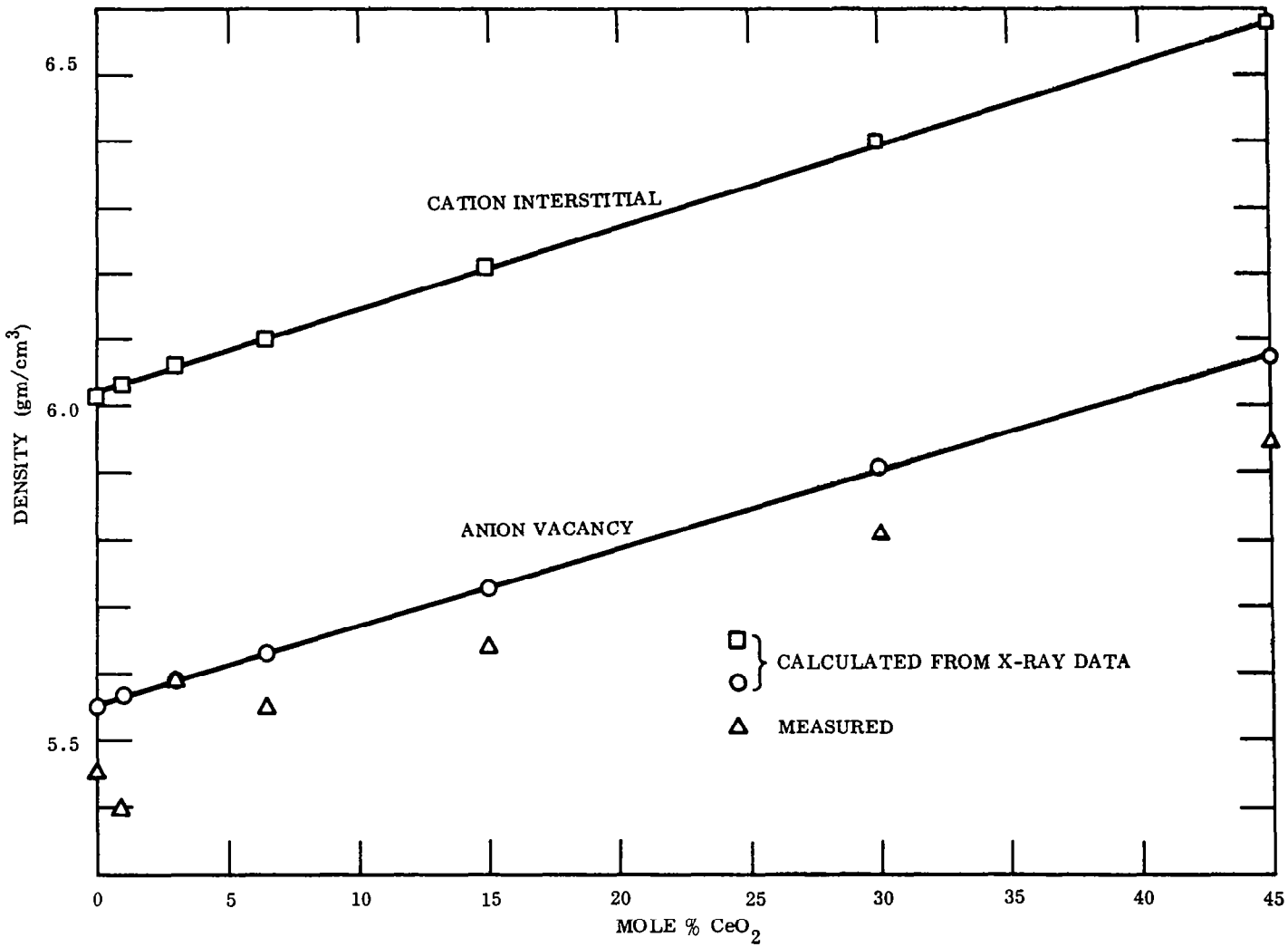

Fig. 2-2 Density of $(ZrO_2)_{0.85-x}(CeO_2)_x(CaO)_{0.15}$ Solid Solutions

Table 2-5

CALCULATED AND MEASURED DENSITIES

Composition (Mole % CeO_2)	Calculated d (gm/cm^3) Interstitial	Vacancy	Experimental d (gm/cm^3)
0	6.01	5.55	5.44
1.0	6.03	5.57	5.40
3.0	6.06	5.59	5.59
6.5	6.10	5.63	5.55
15.0	6.21	5.73	5.64
30.0	6.40	5.91	5.81
45.0	6.58	6.08	5.95

specimens containing no ceria and 1.0 mole % ceria were more difficult to grind to a powder than specimens containing more ceria. In turn the densities of these powders versus theoretical were much lower than for the others. Density measurements for these two compositions were repeated on sintered powders with more careful and longer grinding. The measured value of the density for the sample with no ceria increased from 5.38 to 5.44 while the 1 mole % ceria sample increased from 5.30 to 5.40. Further grinding of these samples may be necessary to eliminate the remaining voids or residual porosity.

For powder samples the densities varied between approximately 97 and 100% of theoretical. Densities obtained on disk specimens from their mass and dimensions indicate porosities between 7 and 15%. In this porosity range there appears to be no correlation between gas permeability and percent porosity at room temperature although the number of interconnecting voids may increase with increasing temperature and duration at temperature. A 3 mole % ceria disk specimen was subjected to sintering conditions of 1500 and 1600 °C for 4 hr and 1775 °C for 3 hr with little change in apparent density of approximately 85% of theoretical for the disk specimen.

2.4 ELECTRICAL CONDUCTIVITY

2.4.1 Experimental Procedure

The electrical conductivity was measured on disk specimens in the composition range 0 to 45 mole % ceria. The disks were 15 to 20 mm in diameter and approximately 1 mm thick. Specimens were sintered at 1600°C for 10 hr. The apparent densities were 85 to 90% of the theoretical calculations. Measurements were made at 1000 cps using a General Radio Impedance Bridge Model 1650A.

Platinum electrodes are prepared by brushing a first coat of Engelhard No. 6926 unfluxed paste on both faces and firing in air for 4 hr at 1000°C. A 6- to 10-cm piece of 5-mil platinum wire in the form of a spiral is then embedded on each face in a second coat of paste and reheated for 4 hr at 1000°C. Twenty-mil platinum wires are then welded to 1- and 2-cm extensions of 5-mil wires on the faces in the disk electrolyte cell assembly. (Figure 2-3.) A final coat of platinum paste is then brushed on, and the assembly is heated in oxygen at 1200°C with passage of 200 mA for 1/2 hr in each direction through the disk sample.

This procedure was used to minimize contact resistance. Kingery et al. (Ref. 29) used spring-loaded platinum blocks, while Tien and Subbarao (Ref. 18) used platinum paste electrodes heat-treated at 1400°C for measurements on $(ZrO_2)_{0.85}(CaO)_{0.15}$. A comparison of conductivities at 1000°C in oxygen taken from the recent literature is shown in Table 2-6.

Table 2-6

COMPARISON OF CONDUCTIVITY DATA AT 1000°C

Sample	Conductivity ($ohm^{-1} cm^{-1}$)	Investigator
$(ZrO_2)_{0.85}(CaO)_{0.15}$	2.6×10^{-2}	Rhodes and Carter (Ref. 30)
	1.5×10^{-2}	Kingery et al. (Ref. (29)
	3.3×10^{-2}	Tien and Subbarao (Ref. (18)
	1.8×10^{-2}	Present work

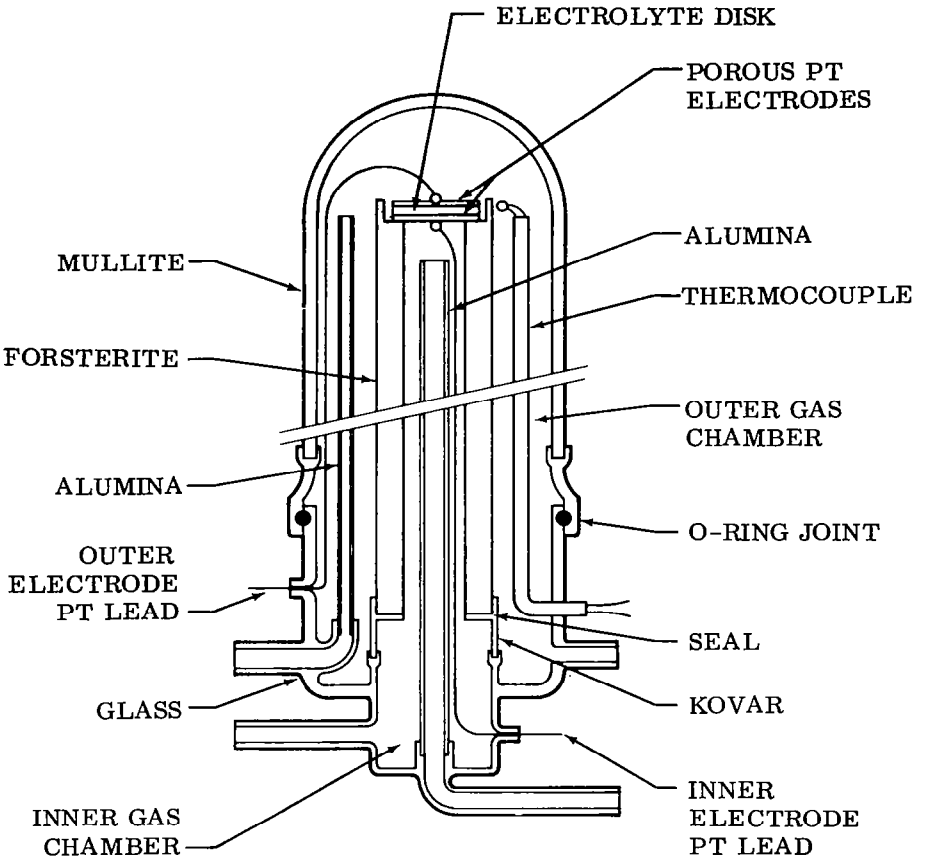

Fig. 2-3 Electrolyte Conductivity Measurement Unit

Despite such factors as purity of materials, density, electrode contact resistance, lead resistance corrections, and order-disorder phenomena that can affect the values, agreement appears to be good.

A gas stream was flowed over the samples at a rate of 10 ml/min. The gas compositions used were oxygen, carbon dioxide containing 0.035% O_2, and 0.92, 1.60, 25.9, and 50.7% CO in CO_2. The temperature interval was 450° to 1200°C. These compositions were analyzed by gas chromatography. For comparison purposes and for determining the oxygen partial pressure of mixtures containing less than 0.92% CO in CO_2 and in 100% CO_2 containing traces of oxygen a $(ZrO_2)_{0.85}(CaO)_{0.15}$ tube cell was constructed to serve as an oxygen gauge (Ref. 31). The gauge was inserted directly into the disk electrolyte cell assembly. The disk specimen on which electrical conductivity measurements were carried out was placed close to the anode surface of the gauge and electrically isolated from it by two short pieces of 20-mil alumina rod (Fig. 2-4). The disk specimen and the oxide cell of the gauge were at the same temperature and the same gas stream bathing the sample flowed past the anode of the oxide cell. The cell voltage was continuously monitored. A 0.92% CO in CO_2 mixture was diluted with 100% CO_2 and fed into the cell.

From the measured EMF and the use of the Nernst equation

$$E = \frac{RT}{4F} \ell n \, P_{O_2}\,(\text{cathode})/P_{O_2}\,(\text{anode}) \qquad (2\text{-}4)$$

the oxygen partial pressure at the anode can be obtained directly, or the CO/CO_2 ratio can be calculated from the measured EMF and the Nernst equation

$$E = E^\circ + \frac{RT}{2F} \ell n \, P_{CO}/P_{CO_2} + \frac{RT}{4F} \ell n \, P_{O_2}\,(\text{cathode}) \qquad (2\text{-}5)$$

Oxygen at one atmosphere was used as the reference pressure at the cathode. E° is the standard value for the CO/CO_2 reaction at the particular temperature and the other symbols have their usual meaning. A calibration of the gauge was made with 1.6%

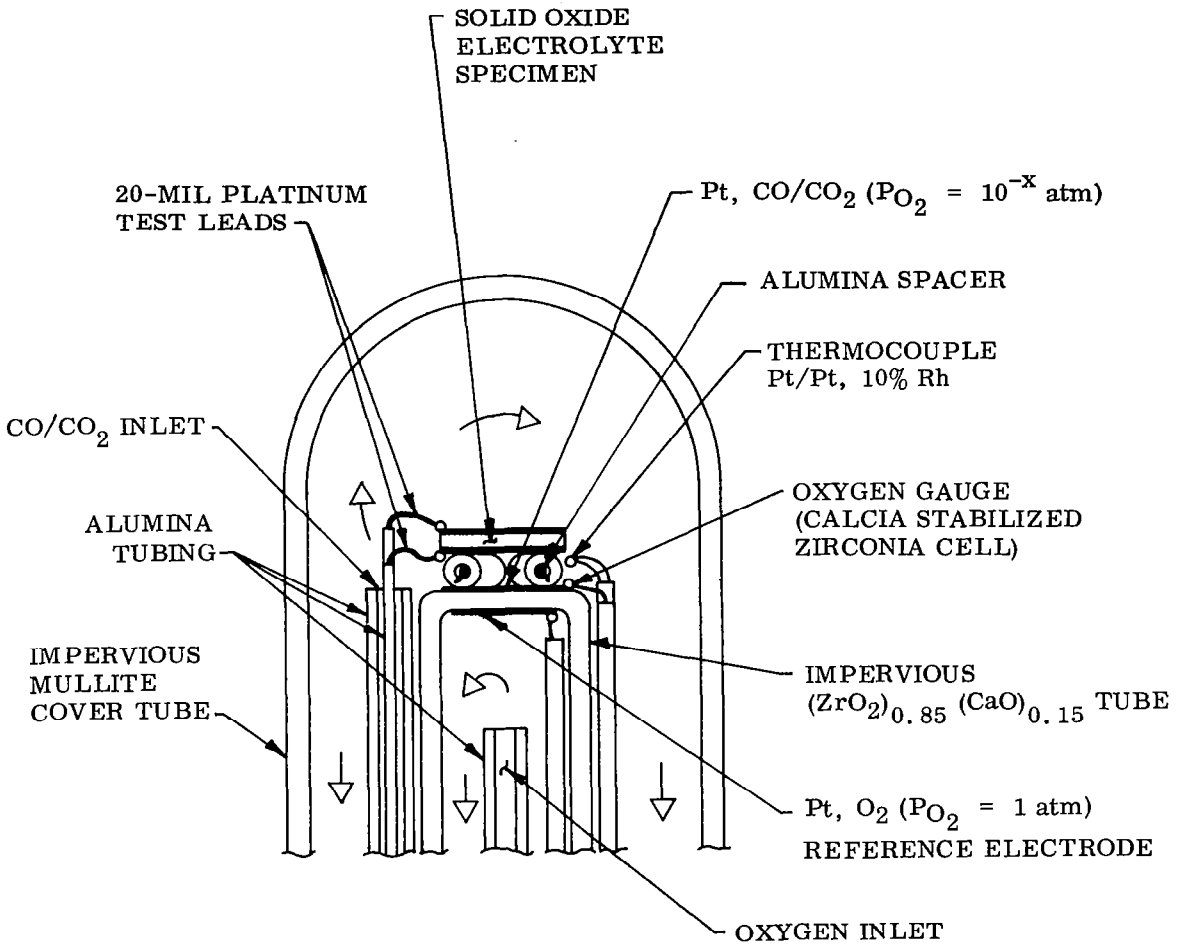

Fig. 2-4 Electrolyte Conductivity Unit With Oxygen Gauge

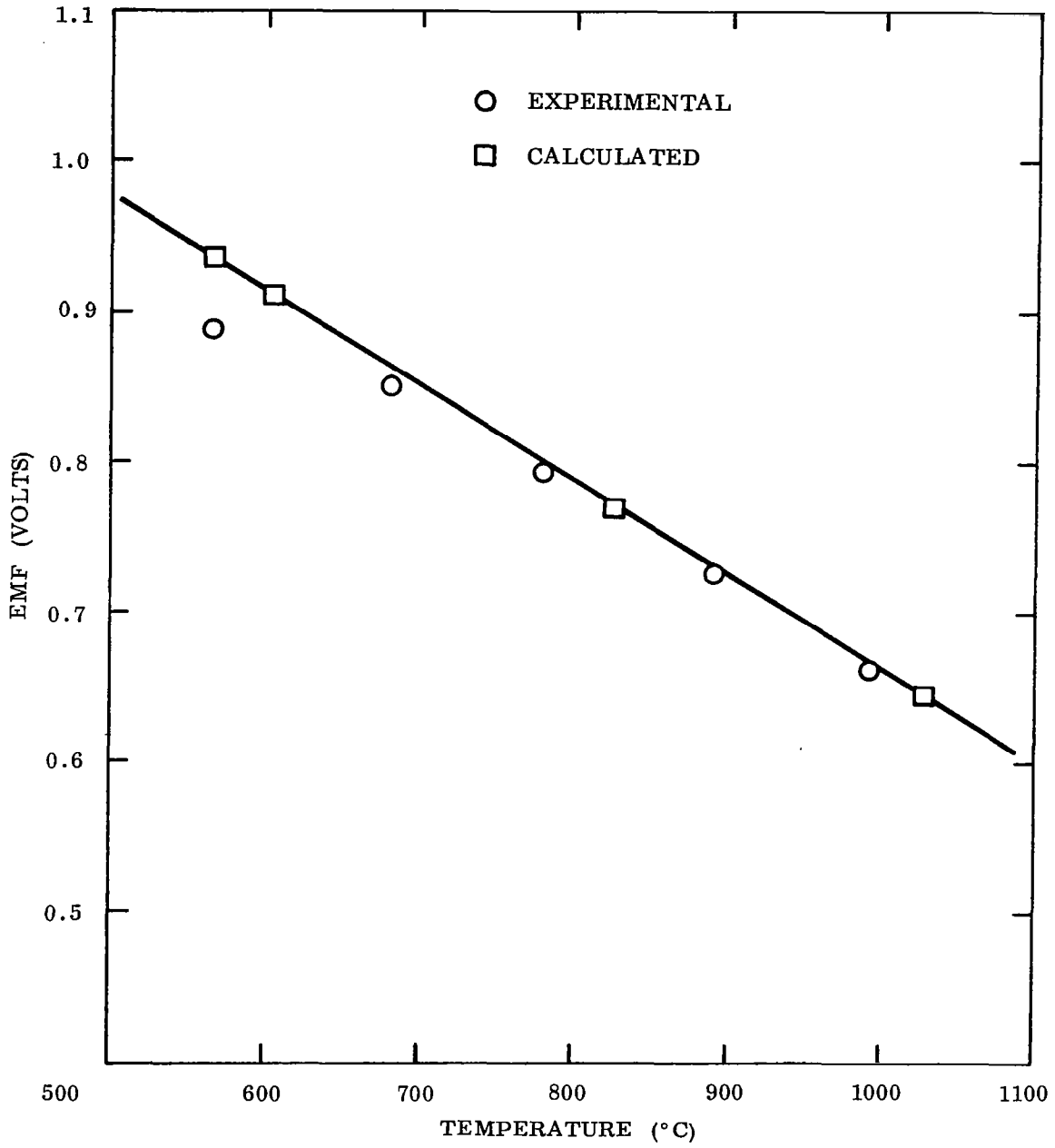

Fig. 2-5 Open-Circuit EMF Values Versus Temperature for the Cell Pt, 1.6% CO in CO_2 $|(ZrO_2)_{0.85}(CaO)_{0.15}|$ O_2, Pt

CO in CO_2 over a temperature range 560−1000°C. The results are shown in Fig. 2-5. At low CO/CO_2 ratios the platinum, CO/CO_2 electrode cannot be used with high accuracy below approximately 700°C. Above 700°C this method can be used to measure the oxygen partial pressures or reducing conditions directly at the sample and at temperature.

The oxide cell and disk specimen were located in the center of the constant temperature zone of the furnace. A 20-mil Pt/Pt, 10% Rh thermocouple placed between the anode and disk served to measure the temperature.

2.4.2 Results

The results are presented as plots of log conductivity versus the reciprocal of the absolute temperature so as to give an over-all picture of the magnitude and temperature dependence of conductivity with respect to ceria concentration and CO/CO_2 composition or oxygen partial pressure. Figures 2-6, 2-7, 2-8, and 2-9 for 6.5, 10, 15, and 30 mole % ceria present this data. For identification of samples only, total ceria is expressed as mole % CeO_2.

The temperature-dependence of the electrical conductivity can be represented by the equation

$$\sigma = A \exp(-Q/kT) \tag{2-6}$$

where

- Q = an energy term
- σ = the measured specific conductivity
- T = the absolute temperature
- k = Boltzmann's constant
- A = a pre-exponential factor

Where a break in the curve occurs with a high-temperature and a low-temperature linear portion, a sum of two terms of the form of Eq. (2-6) is required.

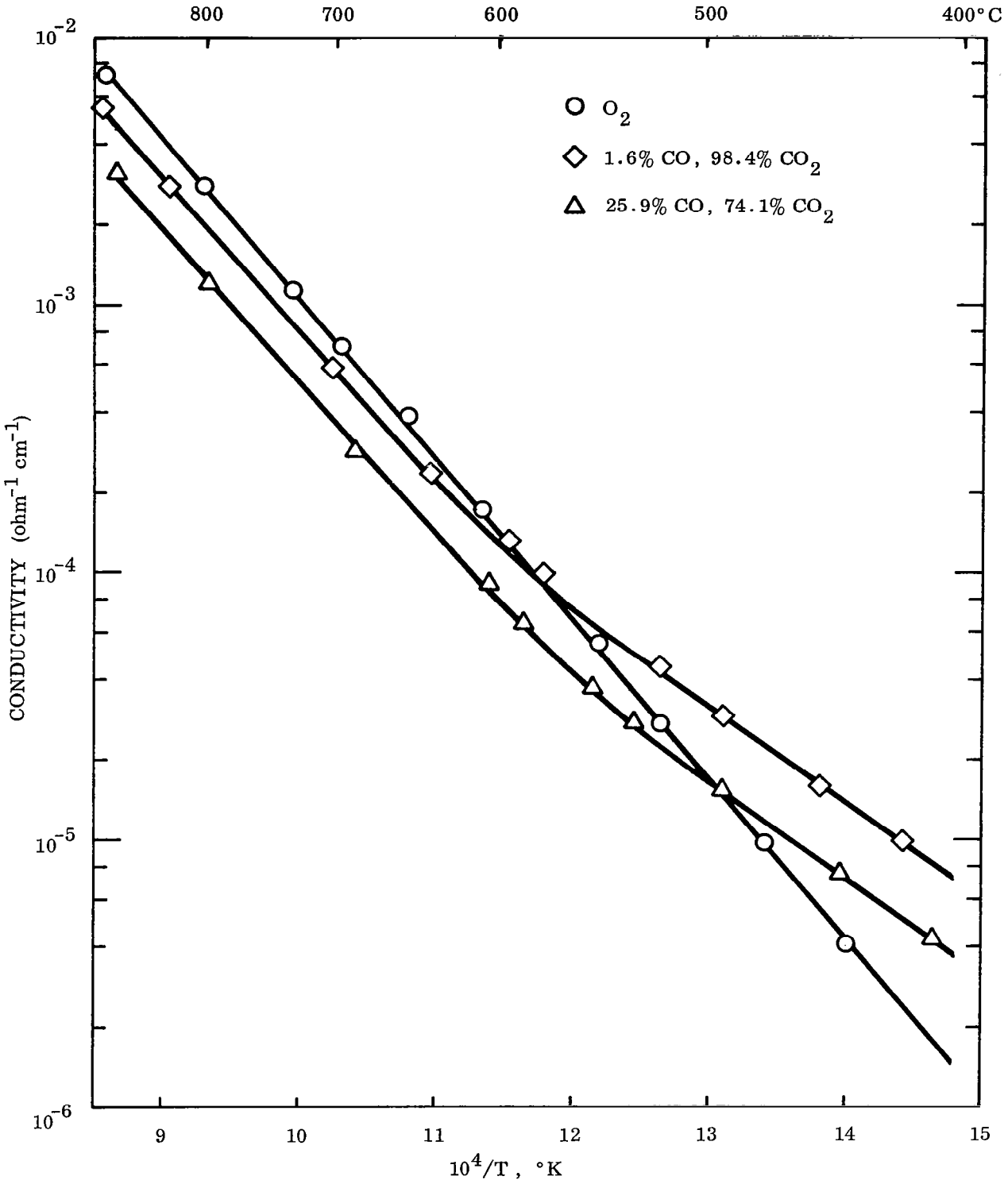

Fig. 2-6 Temperature Dependence of Conductivity for the Solid Solution $(ZrO_2)_{0.785}(CeO_2)_{0.065}(CaO)_{0.15}$

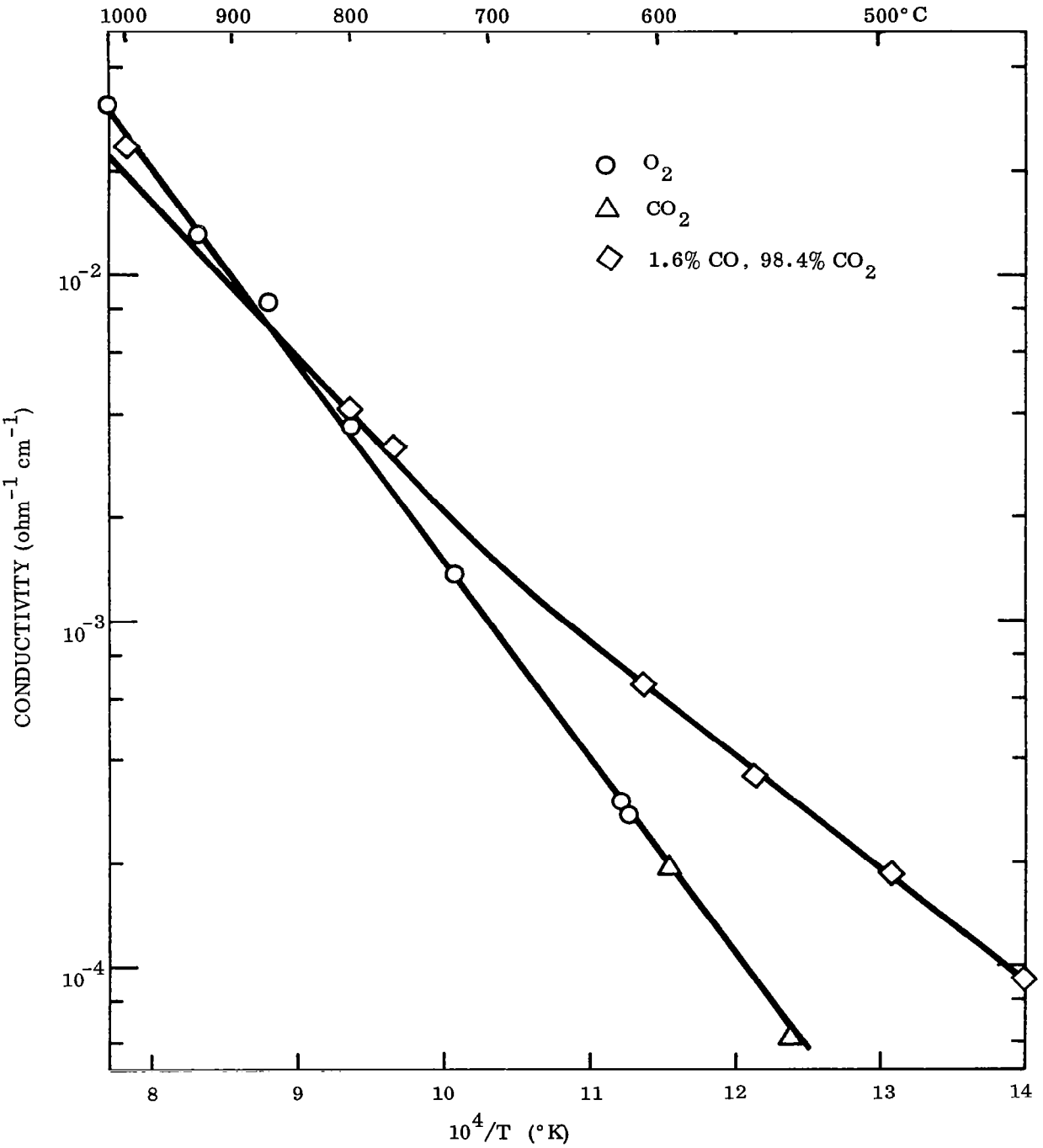

Fig. 2-7 Temperature Dependence of Conductivity for the Solid Solution $(ZrO_2)_{0.75}(CeO_2)_{0.10}(CaO)_{0.15}$

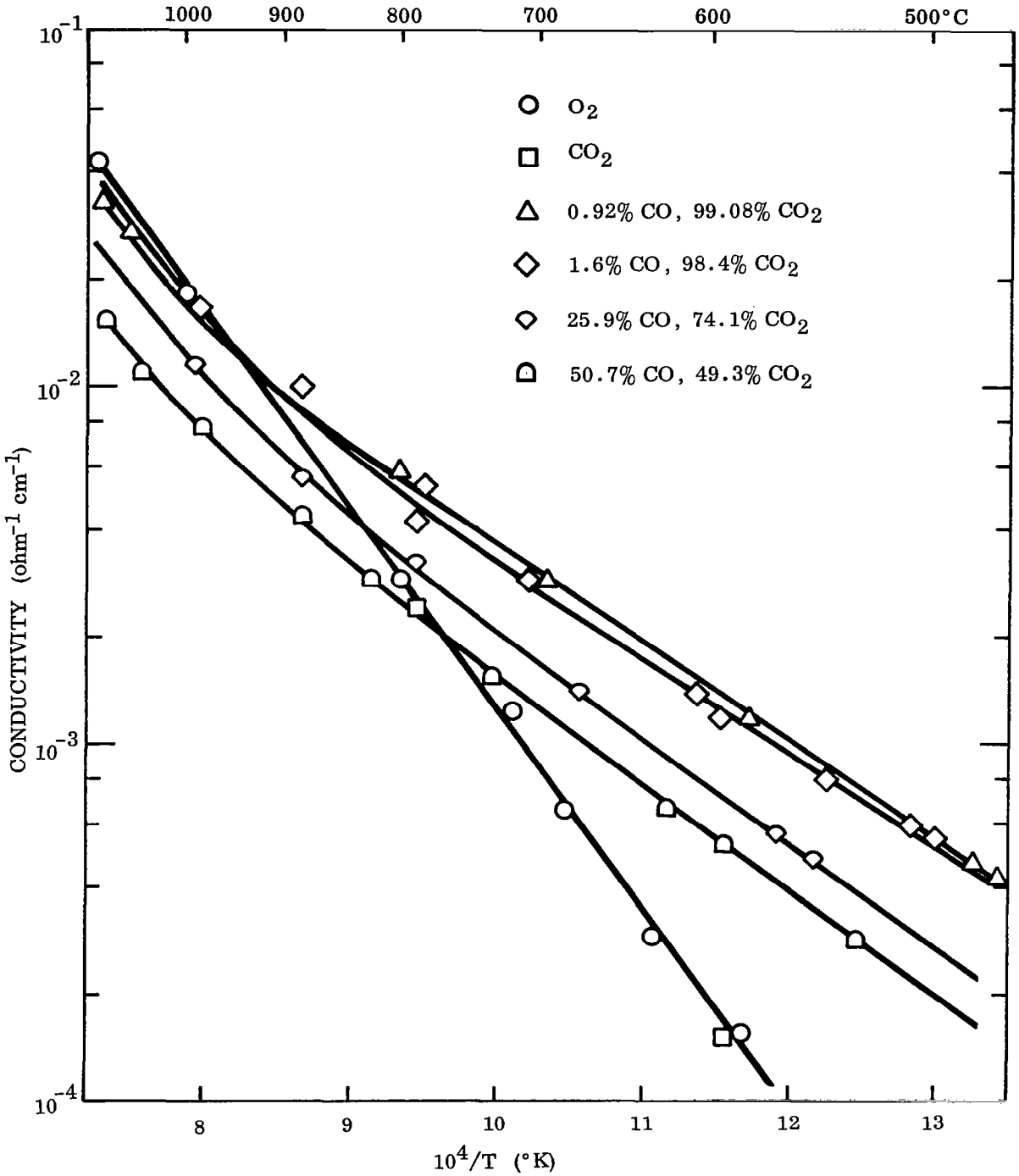

Fig. 2-8 Temperature Dependence of Conductivity for the Solid Solution $(ZrO_2)_{0.70}(CeO_2)_{0.15}(CaO)_{0.15}$

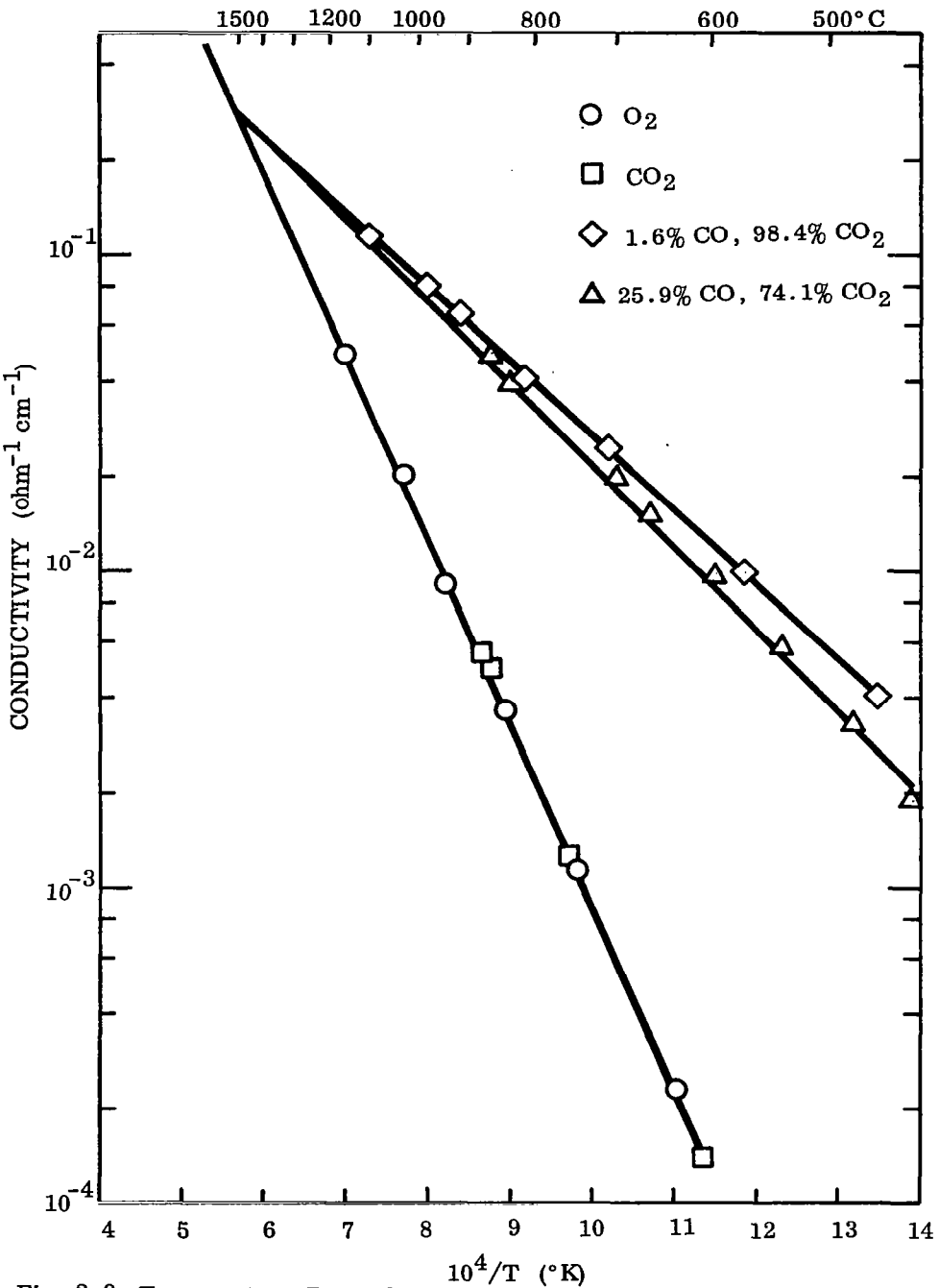

Fig. 2-9 Temperature Dependence of Conductivity for the Solid Solution $(ZrO_2)_{0.55}(CeO_2)_{0.30}(CaO)_{0.15}$

An analysis of the curves for 6.5, 10, 15 and 30 mole % ceria samples (Figs. 2-6 to 2-9) as well as for 0, 3.0, and 45 mole % ceria samples (not shown) was made in accordance with Eq. (2-6) and is shown in Table 2-7.

Table 2-7

CONDUCTIVITY-TEMPERATURE DATA

Mole % CeO_2	Gas Composition	σ (High Temperature)	σ (Low Temperature)
0	O_2	$453 \exp\left(-\frac{1.11}{kT}\right)$	$453 \exp\left(-\frac{1.11}{kT}\right)$
3.0	O_2	$630 \exp\left(-\frac{1.11}{kT}\right)$	$630 \exp\left(-\frac{1.11}{kT}\right)$
6.5	O_2	$1406 \exp\left(-\frac{1.21}{kT}\right)$	$1406 \exp\left(-\frac{1.21}{kT}\right)$
6.5	1.60% CO in CO_2	$297 \exp\left(-\frac{1.10}{kT}\right)$	$1.24 \exp\left(-\frac{0.70}{kT}\right)$
6.5	25.9% CO in CO_2	$110 \exp\left(-\frac{1.06}{kT}\right)$	$0.767 \exp\left(-\frac{0.71}{kT}\right)$
10	O_2	$630 \exp\left(-\frac{1.12}{kT}\right)$	$630 \exp\left(-\frac{1.12}{kT}\right)$
10	1.6% CO in CO_2	–	$2.75 \exp\left(-\frac{0.63}{kT}\right)$
15	O_2	$476 \exp\left(-\frac{1.11}{kT}\right)$	$476 \exp\left(-\frac{1.11}{kT}\right)$
15	3.5×10^{-2}% O_2 in CO_2	$476 \exp\left(-\frac{1.11}{kT}\right)$	$476 \exp\left(-\frac{1.11}{kT}\right)$
15	0.92% CO in CO_2	$53.3 \exp\left(-\frac{0.87}{kT}\right)$	$1.40 \exp\left(-\frac{0.53}{kT}\right)$
15	1.60% CO in CO_2	$53.3 \exp\left(-\frac{0.87}{kT}\right)$	$1.40 \exp\left(-\frac{0.525}{kT}\right)$
15	25.9% CO in CO_2	$48.5 \exp\left(-\frac{0.90}{kT}\right)$	$1.39 \exp\left(-\frac{0.564}{kT}\right)$
15	50.7% CO in CO_2	$14.3 \exp\left(-\frac{0.81}{kT}\right)$	$1.03 \exp\left(-\frac{0.60}{kT}\right)$
30	O_2	$518 \exp\left(-\frac{1.14}{kT}\right)$	$518 \exp\left(-\frac{1.14}{kT}\right)$
30	3.5×10^{-2}% O_2 in CO_2	$518 \exp\left(-\frac{1.14}{kT}\right)$	$518 \exp\left(-\frac{1.14}{kT}\right)$
30	1.60% CO in CO_2	–	$5.96 \exp\left(-\frac{0.47}{kT}\right)$
45	O_2	$385 \exp\left(-\frac{1.12}{kT}\right)$	$385 \exp\left(-\frac{1.12}{kT}\right)$

Tien and Subbarao (Ref. 18) in their study of the zirconia-calcia system reported that at 1000° C with increasing CaO content from 13 to 22 mole % the electrical conductivity decreased from 5×10^{-2} to 6×10^{-3} $ohm^{-1} cm^{-1}$ and the activation energy increased from 1.11 to 1.35 eV. They ascribed the decrease in conductivity to an increase in activation energy for conduction (decrease in carrier mobility) due to the increased size of the cation between which the oxygen ion as charge carrier has to pass when the Zr^{+4} ion (0.92Å) is replaced by the Ca^{+2} ion (1.10Å).

Replacement of the Zr^{+4} ion by the Ce^{+4} ion (1.07Å) over a composition range of 0 – 45 mole % ceria resulted in a small decrease of conductivity at 1000° C in O_2 at 1 atm pressure (Table 2-8) but in contrast to the results of Tien and Subbarao (Ref. 18) the activation energy for ionic conduction remained constant (Table 2-7 and Fig. 2-10). The variation in conductivity appears to be associated with experimental error and not to any cation size effect.

Table 2-8

CERIA CONTENT AND IONIC CONDUCTIVITY AT 1000° C AND P_{O_2} = 1 ATM

Sample (mole % ceria)		Conductivity ($ohm^{-1}cm^{-1}$) $\sigma \times 10^2$	Average value $\sigma \times 10^2$
0		1.9	
3		2.5	
6.5		2.3	
15	No. 1	1.9	1.9 ± .4
15	No. 2	1.5	
30		1.5	
45		1.4	

Figure 2-11 shows the dependence of conductivity on oxygen partial pressure for a 15 mole % ceria sample at constant temperature. The dependence of conductivity on mole % ceria (in 1.6% CO in CO_2) at constant temperature is brought out in Fig. 2-12.

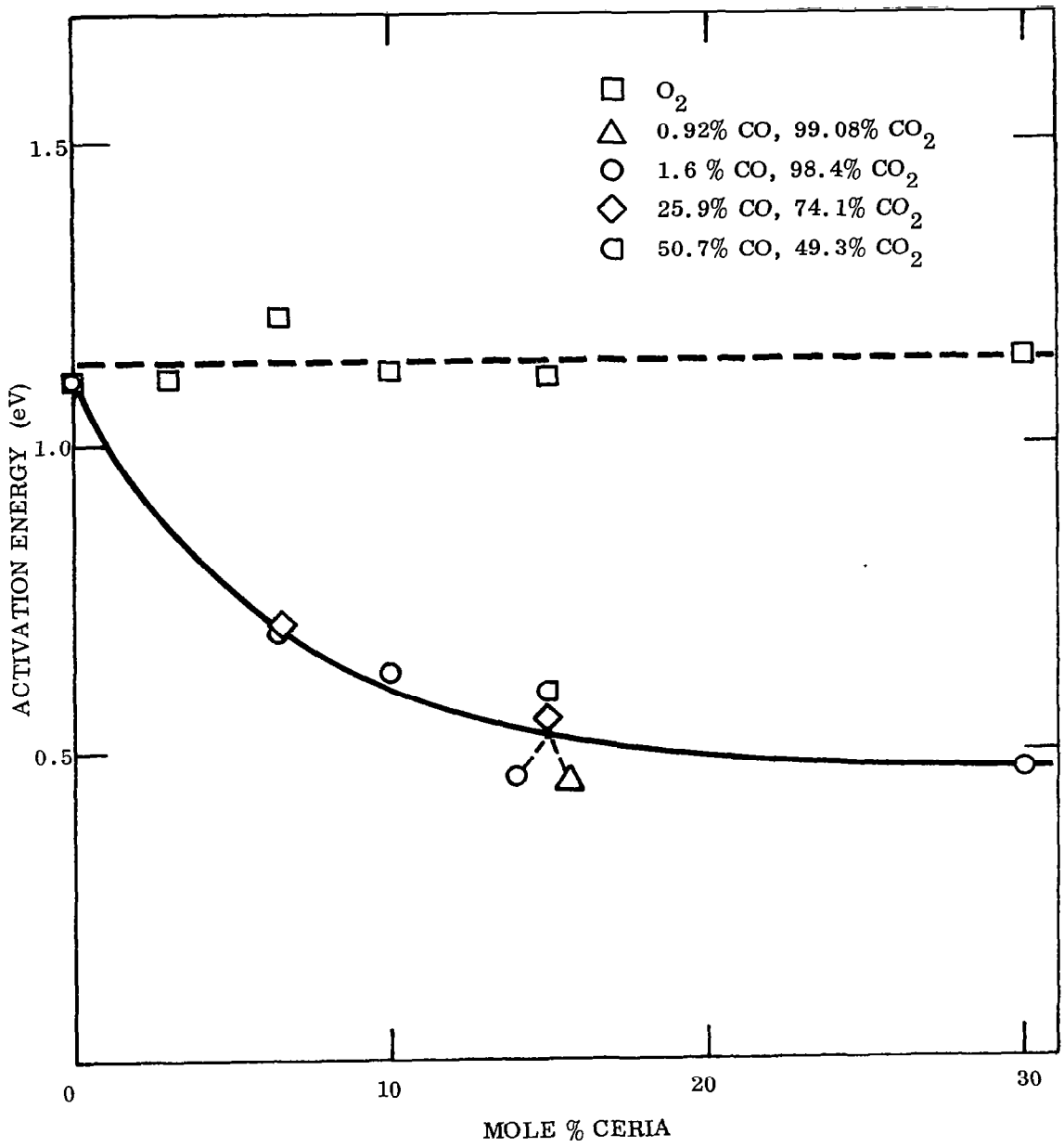

Fig. 2-10 Composition Dependence of Activation Energy for (—) Electronic and (– –) Ionic Conduction in $(ZrO_2)_{0.85-x}(CeO_2)_x(CaO)_{0.15}$

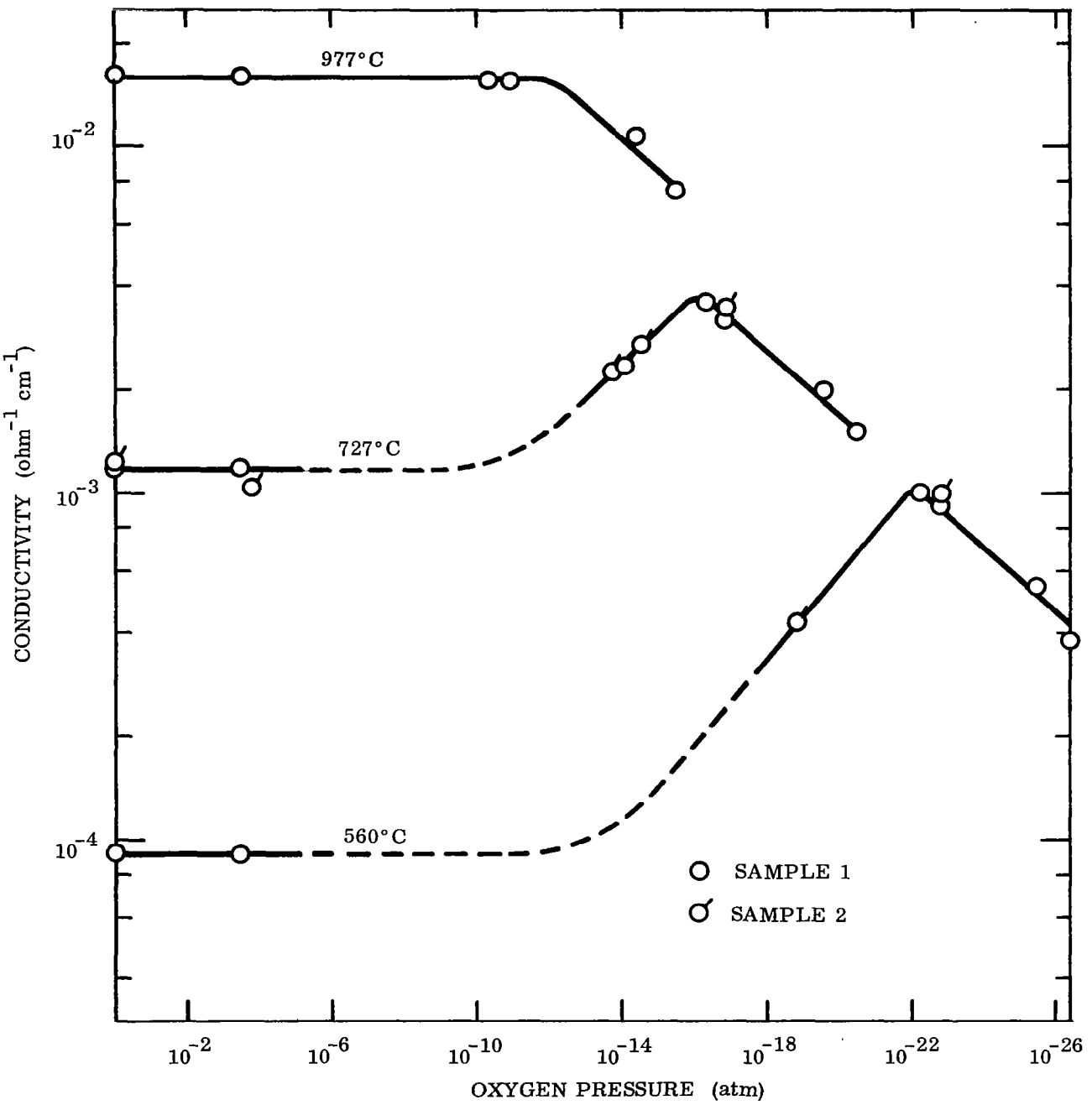

Fig. 2-11 Oxygen Partial Pressure Dependence of Conductivity at Constant Temperature for the Solid Solution $(ZrO_2)_{0.70}(CeO_2)_{0.15}(CaO)_{0.15}$

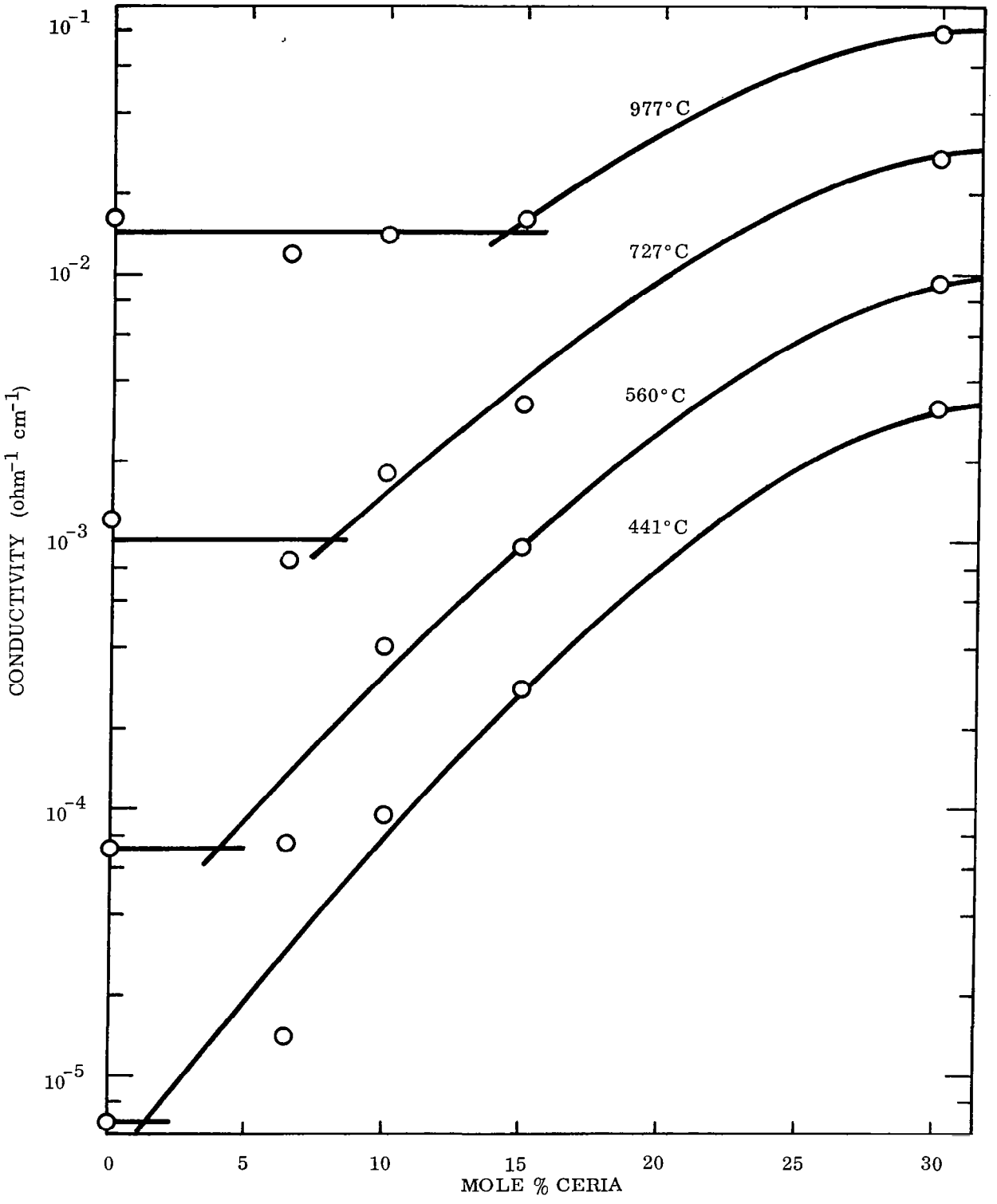

Fig. 2-12 Dependence of Conductivity on Mole Percent Ceria in $(ZrO_2)_{0.85-x}(CeO_2)_x(CaO)_{0.15}$ at Indicated Temperatures in 1.6% CO-98.4% CO_2

The conductivity results can be summarized as follows:

When the oxygen (P_{O_2} = 1 atm) and carbon dioxide ($P_{O_2} \cong 10^{-3}$ atm) curve is taken as the reference line, the conductivity curves for each $CO-CO_2$ gas mixture appear to have two approximately linear portions, a high-temperature portion below and a low-temperature portion above the reference line. In both portions of the curve, the conductivity decreases with increasing %CO, starting from 0.92% CO. In contrast, in going from O_2 (or CO_2) to 0.92% CO, there is a small decrease in conductivity in the high-temperature region and a pronounced increase in conductivity in the low-temperature region. The temperatures at which the break in the high- and low-temperature portions of the $CO-CO_2$ conductivity curves occur, and the temperatures at which the $CO-CO_2$ conductivity curves intersect the O_2 reference line, are primarily dependent on the mole % ceria in the solid solution and secondarily on the CO/CO_2 ratio (%CO) or oxygen partial pressure.

An interpretation of these results is given after presentation of the experimental results of the study of the disorder equilibrium in the ceria solid solutions used in the conductivity study.

2.5 DISORDER EQUILIBRIUM

2.5.1 Experimental Procedure

Results reported in the previous sections on the preparation and characterization of the system $(ZrO_2)_{0.85-x}(CeO_2)_x(CaO)_{0.15}$ from 0 to 45 mole % ceria have shown that in this composition range solid solutions are formed having the fluorite-type defect structure with the concentration of oxygen ion vacancies in the anion sublattice remaining at 15 mole % similar to that found in the absence of ceria in $(ZrO_2)_{0.85}(CaO)_{0.15}$. In the $(ZrO_2)_{0.85}(CaO)_{0.15}$ solid solution, the oxygen ion vacancy concentration is independent of temperature and oyxgen partial pressure, and is controlled only by the composition, i.e., mole % CaO. In contrast, in the ceria-containing solid solutions, because of the relative ease of reduction of CeO_2 to $CeO_{1.5}$ or (Ce^{+4} to Ce^{+3}), a disorder equilibrium involving oxygen ion vacancies, excess electrons, and

other structure defects is expected to exist depending on the mole % ceria, partial pressure of oxygen, and temperature. The type and number of ionic and electronic defects and their temperature and oxygen pressure dependence, profoundly affects the magnitude and temperature dependence of conductivity, the electron and ion transport numbers, and other electrochemical properties of interest in the use of these solid solutions as electrolytes in the electrolysis of CO_2 and CO_2-H_2O mixture. Disorder equilibria data involving ceria solutions in this composition range in zirconia-calcia or other oxide systems are not available in the literature. Measurements of composition changes and the CeO_2–$CeO_{1.5}$ equilibrium as a function of oxygen partial pressure and temture were undertaken using a microweighing technique.

The experimental arrangement is shown in Fig. 2-13. The samples consisted of 30, 15 and 6.5 mole % ceria disks of approximately 1 – 2 mm thickness and 1.5 cm diameter. An ultrasonic drill was used to cut a small hole near the edge of each disk sample which was subsequently cleaned and dried in an oven. The sample was suspended from the beam of a Cahn RG Electrobalance into a quartz hang-down tube by means of a platinum wire. A tare weight was attached on the other end of the beam. A platinum/platinum 10% rhodium thermocouple was positioned near the disk sample. An icebath was used as the reference junction. A resistance-heated furnace surrounded the quartz tube. The precision of the temperature measurements is estimated to be ±2°. The whole system containing the balance and sample was purged by evacuating and filling several times with the required gas. The gas was then adjusted to flow at a rate of about 5 ml/min circulating directly to the sample through a quartz side tube and then through the rest of the 2 to 3 liter system. Tank oxygen and CO-CO_2 mixtures were used. A typical reduction curve for 15 mole % ceria using 25.9% CO in CO_2 is shown in Fig. 2-14. The curve for the reoxidation of this sample is shown in Fig. 2-15. A small zero point shift upward of about 0.1 mg above the room temperature value can be seen in these figures. All weight loss values have been corrected for this effect. The approximate furnace heating and cooling rates can be gauged from the time notations in Figs. 2-14 and 2-15. For some samples the temperature was kept constant for a period of time at several points to determine if equilibrium had been attained. For one sample, 6.5 mole % CeO_2 at 1000°C, the equilibrium point was approached by means of reduction and by means of oxidation and the same value

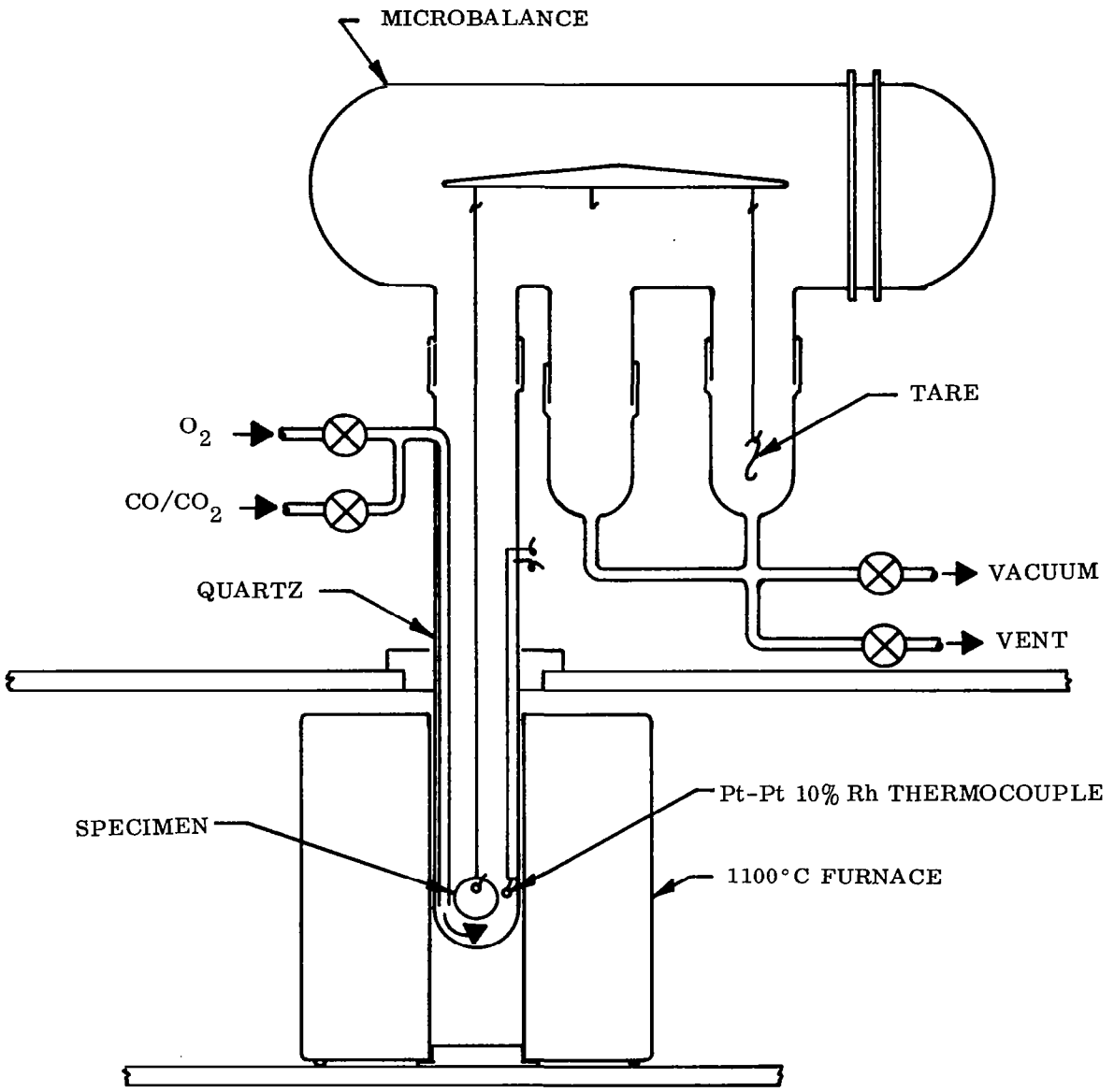

Fig. 2-13 Microweighing Assembly

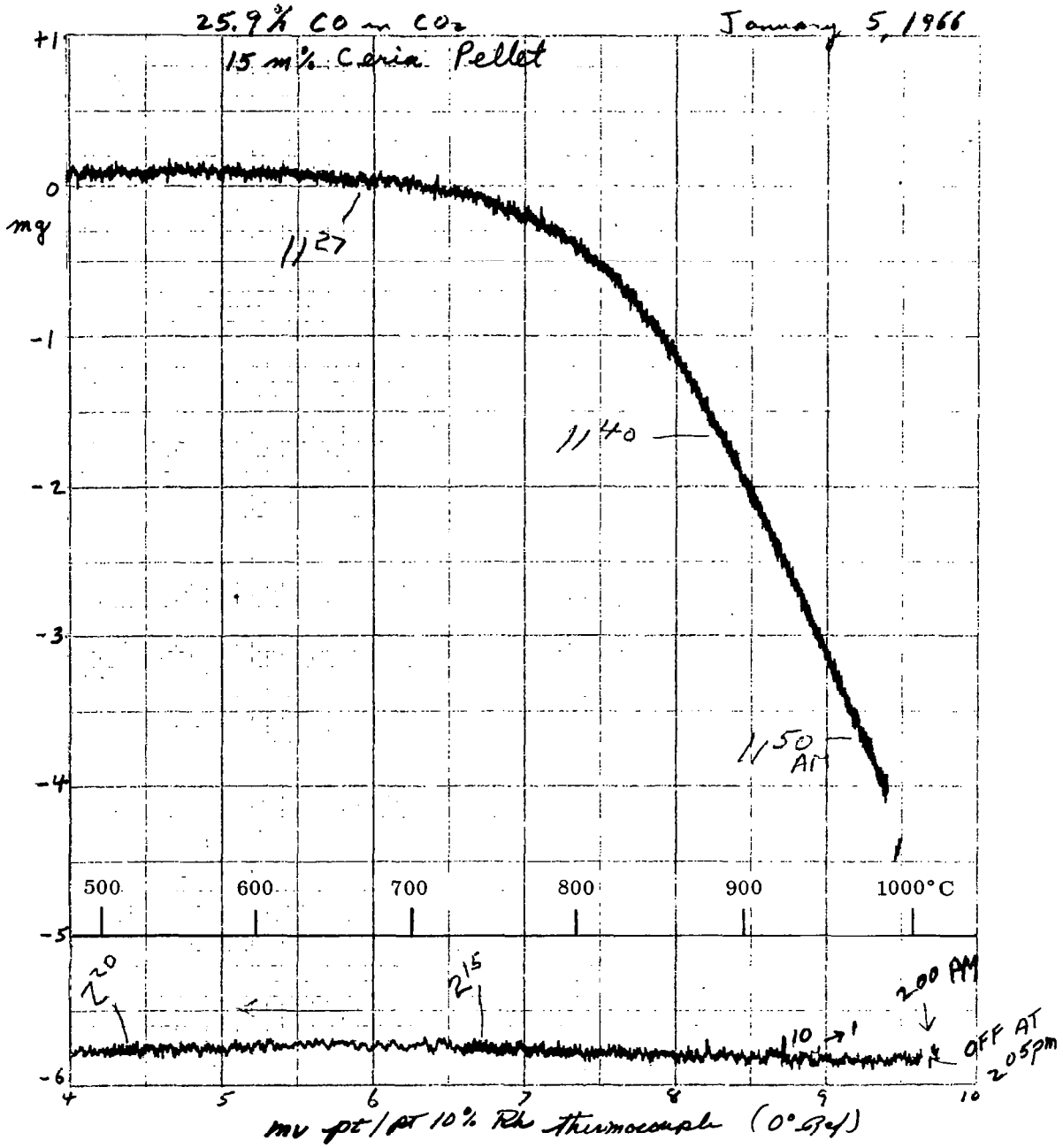

Fig. 2-14 Reduction of a Ceria Sample

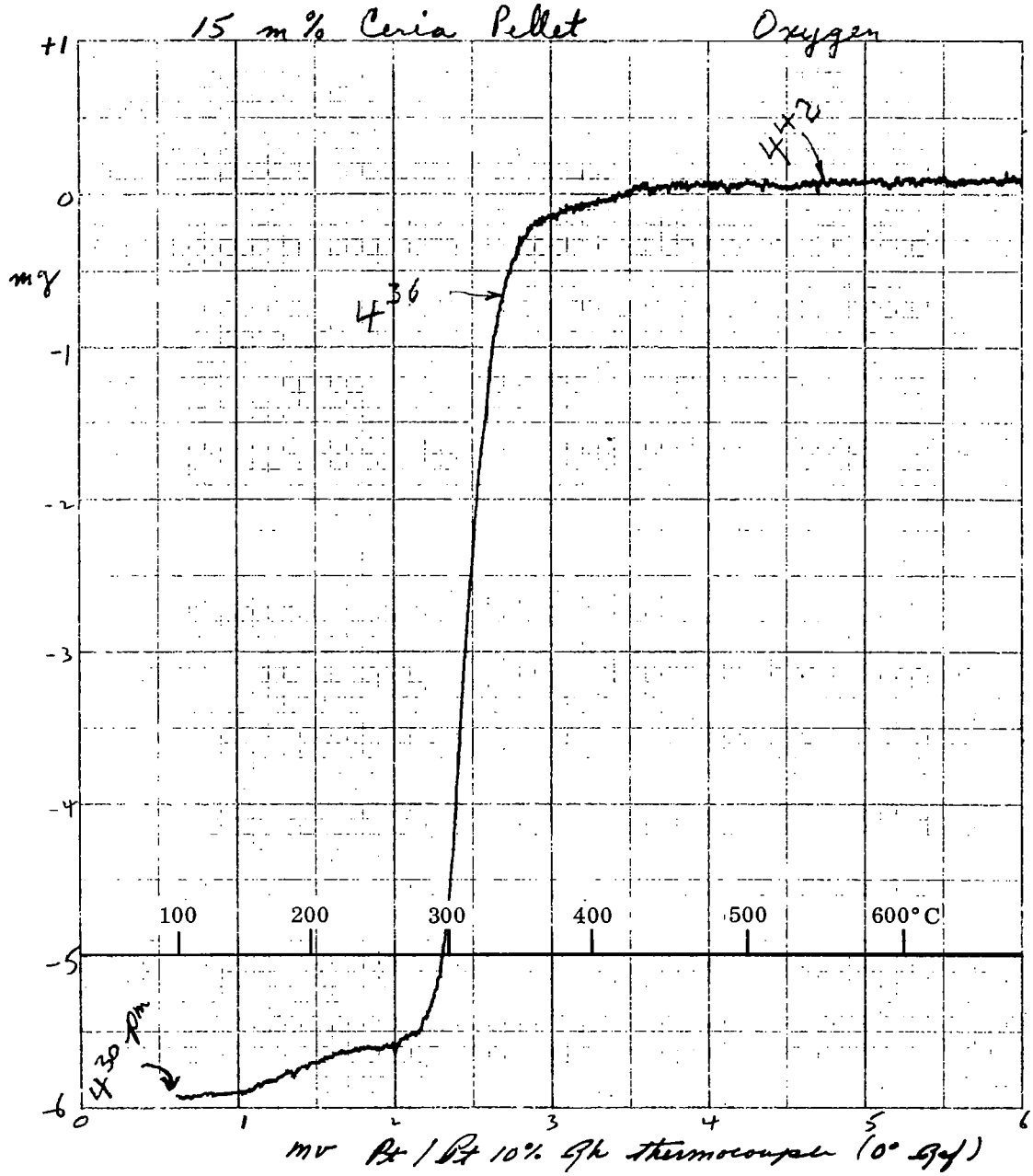

Fig. 2-15 Oxidation of a Ceria Sample

1.30 ± 0.05 mg was obtained. The error as a fraction of the total weight change for this value was 4%. The precision of the weight change measurements was ± 0.05 mg. The error as a fraction of total weight change for all other weight change measurements was 2% or less.

2.5.2 Results

Microweighing

The microweighing runs are presented in chronological order for samples 6.5, 15, and 30 mole % ceria in Tables 2-9, 2-10, and 2-11. Shown are the sample weight, gas composition, observed weight loss, time at temperature and % weight loss or degree of reduction to $CeO_{1.5}$.

Reduced samples were always reoxidized to their original weight so that possible loss of volatile oxide species was excluded. It may therefore be assumed that in the reduction-oxidation process at temperatures of 1000°C or less the exchange of oxygen with the crystal lattice occurs according to the over-all reaction

$$CeO_2 + \frac{1}{2} CO \rightleftharpoons CeO_{1.5} + \frac{1}{2} CO_2 \qquad (2\text{-}7)$$

or

$$CeO_{1.5} + \frac{1}{4} O_2 \rightleftharpoons CeO_2 \qquad (2\text{-}8)$$

The equilibrium weight loss values taken from Tables 2-9, 2-10, and 2-11 are recalculated (Table 2-12) in terms of oxygen partial pressure, temperature, original $(CeO_2)_x$ values and equilibrium CeO_2 and $CeO_{1.5}$ values where

$$(CeO_2)_y + (CeO_{1.5})_z = (CeO_n)_x \qquad (2\text{-}9)$$

Table 2-9

OBSERVED WEIGHT LOSS[a] IN THE REDUCTION OF CERIUM DIOXIDE IN MIXED OXIDE SOLID SOLUTIONS AT 1000° C

Composition: $(CeO_2)_{0.065}(ZrO_2)_{0.785}(CaO)_{0.15}$

Sample weight: 756.5 mg

Calculated weight loss to $CeO_{1.5}$: 3.40 mg

Run	% CO in CO_2	Time at temperature (min)	Weight loss (mg)	Weight loss[b] (%)
1,2 3[d]	25.9	(c)	1.45	
4 5[d]	25.9	(c)	1.80	
6 7[d]	25.9	(c)	2.50	
8 9[d]	25.9	120	2.85	83.8
10 11[d]	0.92	220	1.30	38.2
12	0.92	175	1.25	36.8
13	49.4	25	3.10	91.2
14[e]	0.92	410	1.35	39.7

(a) No weight change was noted for reduced samples from cooling curves similar to the one shown in Fig. 2-14.
(b) Percent weight loss is equivalent to degree of reduction for CeO_2 to $CeO_{1.5}$
(c) Furnace was turned off when 1000° C was reached.
(d) Reoxidized to cerium dioxide in 1 atm of oxygen as in Fig. 2-15.
(e) Reoxidized from a weight loss of 3.05 mg in 49.4% CO in Run 13 to 1.35 mg in Run 14.

Table 2-10

OBSERVED WEIGHT LOSS IN THE REDUCTION OF CERIUM DIOXIDE IN MIXED OXIDE SOLID SOLUTIONS BY 25.9% CO IN CO_2

Composition: $(CeO_2)_{0.15}\ (ZrO_2)_{0.70}\ (CaO)_{0.15}$

Sample weight: 782.9 mg

Calculated weight loss to $CeO_{1.5}$: 7.78 mg

Run	t (° C)	Time at temperature (min)	Weight loss, (mg)	Weight loss (%)
1	1000	5	5.95	76.5
	790	(b)	5.90(b)	75.8
	590	(b)	5.80(b)	74.6
2(a)				
3	1000	106	6.05	77.8
	790	(b)	5.90(b)	75.8
	590	(b)	5.80(b)	74.6
4(a)				
5	1000	13	6.00	77.1
	790	(b)	5.90(b)	75.8
	590	(b)	5.80(b)	74.6

(a) Reoxidized to cerium dioxide in one atmosphere of oxygen.
(b) These values taken from cooling curves where sample may not have attained equilibrium are not as reliable as the 1000° C values.

Table 2-11

OBSERVED WEIGHT LOSS IN THE REDUCTION OF CERIUM DIOXIDE IN MIXED OXIDE SOLID SOLUTIONS

Composition: $(CeO_2)_{0.30}\ (ZrO_2)_{0.55}\ (CaO)_{0.15}$

Sample weight: 607.3 mg

Calculated weight loss to $CeO_{1.5}$: 11.40 mg

Run	% CO in CO_2	Temperature (°C)	Time at temperature (min)	Weight loss (mg)	Weight loss (%)
1	25.9	790	(a)	6.45	
2(b)					
3	25.9	1000	(a)	6.75	59.2
		790		6.45(c)	56.6
		590		6.15(c)	53.9
4(b)					
5	0.92	1000	47	4.10	36.0
		790	20	3.90	34.3
		590	30	3.60	31.6
6	0.92	1000	214	4.05	35.6
		790	45	3.85	33.8
		590	30	3.65	32.3
7(b)					
8	49.4	1000	(a)	7.30	64.0
		790		7.00(c)	61.4
		590		6.60(c)	57.9
9	49.4	1000	50	7.80	68.4
		790		7.60(c)	66.7
		590		7.30(c)	64.0
10	49.4	1000	(a)	7.85	68.9

(a) Furnace shut off at 1000°C.
(b) Reoxidized to cerium dioxide in one atmosphere of oxygen.
(c) Taken from cooling curves.

Table 2-12

THE CeO_2-$CeO_{1.5}$ EQUILIBRIUM IN THE REDUCTION OF $(CeO_2)_x(ZrO_2)_{0.85-x}(CaO)_{0.15}$ SOLID SOLUTIONS

$(CeO_2)_x$	Equilibrium values			Temperature (° C)	-log P_{O_2} (atm)	
	$(CeO_2)_y$	$(CeO_{1.5})_z$	CeO_n			
0.30	0.192	0.109	1.819	1000	9.95	0.92% CO in CO_2
	0.198	0.102	1.827	790	14.5	
	0.203	0.097	1.838	590	20.9	
0.30	0.121	0.179	1.701	1000	13.1	25.9% CO in CO_2
	0.128	0.172	1.714	790	17.7	
	0.136	0.164	1.728	590	24.2	
0.30	0.091	0.209	1.652	1000	14.1	49.4% CO in CO_2
	0.098	0.202	1.663	790	18.6	
	0.106	0.194	1.677	590	25.0	
0.15	0.033	0.117	1.611	1000	13.1	
0.065	0.040	0.025	1.809	1000	9.95	
	0.011	0.054	1.581	1000	13.1	
	0.006	0.059	1.544	1000	14.1	

Table 2-13

THE CeO_2-$CeO_{1.5}$ EQUILIBRIUM IN THE REDUCTION OF CeO_2 AT 1000° C[(a)]

$(CeO_2)_y$	$(CeO_{1.5})_z$	CeO_n	-log P_{O_2} (atm)
0.70	0.30	1.85	16.5
0.60	0.40	1.80	18.2
0.46	0.54	1.73	20.3
0.34−0	0.66−1.00	1.67−1.50	20.8

(a) Reference 33.

For purposes of comparison, several CeO_2-$CeO_{1.5}$ equilibrium points for the reductoin of 100 mole % ceria at 1000°C taken from the work of Brauer et al. (Ref. 33) are tabulated in Table 2-13. The values in Table 2-13 and the 1000°C values in Table 2-12 are plotted in Fig. 2-16 showing the overall oxygen content in CeO_n in equilibrium with the oxygen partial pressure for 6.5, 15, 30 and 100 mole % ceria. It is obvious from Fig. 2-16 that a large increase in the equilibrium oxygen partial pressure occurs in going from 100% ceria to 6.5−30 mole % ceria solid solutions.

For 100 mole % ceria the solid solution range of CeO_n extends to n = 1.67 and two phases coexist from n = 1.67 to 1.50. In the reduction of the ceria dissolved in the zirconia-calcia solid solutions the solid solution for CeO_n appears to extend to n = 1.50. The solid solution range for CeO_n can be deduced from the oxygen partial pressure dependence on n in CeO_n. The phase relationship in pure ceria obtained by Brauer et al. (Refs. 32,33) from oxygen equilibrium pressure measurements and high temperature x-ray diffraction studies extends to ~650°C. Below ~650°C, a more complicated phase relationship is present in 100 mole % ceria. In contrast, our oxygen equilibrium data for ceria dissolved in zirconia-calcia solid solutions indicates that the solid solution fluorite-type one phase region for values of n to 1.50 appears to extend to room temperature.

Lattice Parameters and Density

The ceria samples reduced in the microbalance apparatus (Section 2.5.1) were subsequently examined by x-rays at room temperature. An additional 30 mole % ceria sample of sufficient size for x-ray and pycnometric density examination was also reduced in the microbalance apparatus according to the method described in Section 2.5.1.

For fully oxidized ceria a single phase solid solution with the fluorite-type structure was found in the 0 − 45 mole % ceria region. From x-ray and pycnometric density measurements it was concluded that the oxygen ion vacancy concentration remains constant at 15 mole %. The increase in lattice parameter with increasing Ce^{+4} concentration was ascribed to the replacement of Zr^{+4} (0.92 Å) by Ce^{+4} (1.07 Å) in the crystal lattice (Section 2.3).

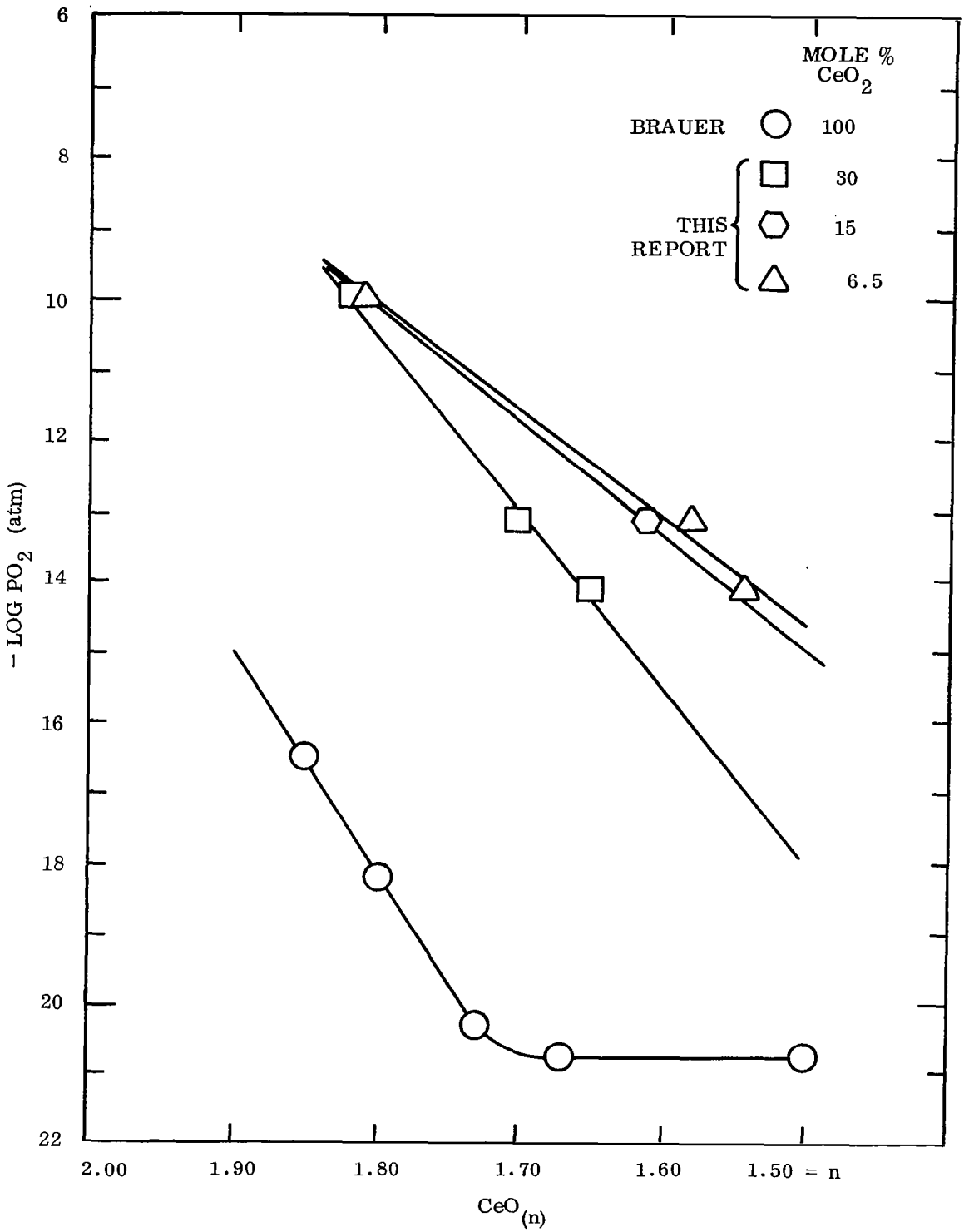

Fig. 2-16 Dependence of Oxygen Partial Pressure on Composition $CeO_{(n)}$ at 1000° C

In the reduction of ceria in the mixed oxide system under examination a further increase of the ionic radius occurs with the replacement of Ce^{+4} with Ce^{+3} (1.18 Å). The lattice parameters for the concentrations examined are presented in Table 2-14. A single phase solid solution with the fluorite-type structure is retained up to the maximum concentration examined – 20.4 mole % $CeO_{1.5}$.

The following analysis was used to correlate the variation of lattice parameter with CeO_2-$CeO_{1.5}$ concentration. The dependence of lattice parameter on mole % CeO_2 in the system $(ZrO_2)_{0.85-x}(CeO_2)_x(CaO)_{0.15}$ (calculated from Fig. 2-1 in Section 2.3) is given by

$$25°C: \quad a_o(\text{Å}) = 5.134 + 0.00338\,y \qquad (z = 0) \tag{2-10}$$

The equivalent equation for the dependence of lattice parameter on mole % $CeO_{1.5}$ in the system CeO_2-$CeO_{1.5}$ [calculated from Bauer et al. Ref. (32)] is

$$20°C: \quad a_o(\text{Å}) = 5.410 + 0.00223\,z \qquad (y + z = 100) \tag{2-11}$$

where

y, z = concentrations of CeO_2, $CeO_{1.5}$ in mole %

0.00338, 0.00223 = constants $\Delta a_o/\Delta y$, $\Delta a_o/\Delta z$

Adding the constant 0.00223 z from Eq. (2-11) to Eq. (2-10) we get

$$a_o = 5.134 + 0.00338\,y + 0.00223\,z \tag{2-12}$$

which was used to obtain the calculated lattice parameters in Table 2-14. The good agreement between calculated and experimental values indicates that in this composition range the solid solutions are approximately ideal, i.e., ΔV mixing $\cong$ O.

To maintain charge neutrality in the mixed oxide crystal one oxygen ion is removed and one oxygen ion vacancy is created in the lattice for every 2 Ce^{+4} ions reduced to Ce^{+3}. Reduction of the 30 mole % ceria sample No. 2 (Table 2-14) should therefore increase

the oxygen vacancy concentration from 15 to 25.2 mole %. The experimental and calculated densities are shown in Table 2-15 for the reduced and fully oxidized 30 mole % ceria sample. Residual porosity in the powder may account for the discrepancy.

Table 2-14

LATTICE PARAMETERS OF $(ZrO_2)_{0.85-x}(CeO_2)_y(CeO_{1.5})_z(CaO)_{0.15}$

Concentration (mole %)			Lattice parameter a_o (Å)	
Total Ceria	CeO_2	$CeO_{1.5}$	Measured	Calculated
6.5	3.1	3.4	5.162 ± 0.003	5.164
15	4.4	10.6	5.212 ± 0.005	5.210
30 No. 1	11.7	18.3	5.280 ± 0.003	5.276
30 No. 2	9.6	20.4	5.283 ± 0.003	5.280

Table 2-15

DENSITIES OF OXIDIZED AND REDUCED 30 mole % CERIA SOLID SOLUTIONS

	Composition (mole %)		Density (gm/cc)	
State of Sample	CeO_2	$CeO_{1.5}$	Calculated (x-ray)	Measured (pycnometric)
Oxidized	30	0	5.91	5.81
Reduced	9.6	20.4	5.69	5.40

2.6 DISCUSSION OF ELECTRICAL CONDUCTIVITY AND DISORDER EQUILIBRIUM

To interpret the results of the conductivity measurements in the CO-CO_2 mixtures, we separate the ionic and electronic contributions to the total conductivity process into two terms

$$\sigma = A\, e^{-Q_i/kT} + B\, e^{-Q_e/kT} \qquad (2\text{-}13)$$

where the Q's are constants over a specified temperature range and characterize the temperature coefficient of the conductivity and A and B are constant pre-exponential terms.

The magnitude and temperature-dependence of conductivity is related to the concentration of defects found in oxide crystals such as vacancies, interstitial ions, excess electrons, and electron holes. Q_i or Q_e, in general, contains a term or terms for the energy required to form these defects, e.g., energy or Helmholtz free energy, and a term for the energy, i.e., activation energy required for their migration or diffusion through the crystal.

Ionic and electronic defects may arise due to thermal disorder resulting in intrinsic electrical conductivity. Ionic defects may be produced by oxidation-reduction, due to interaction of the oxide crystal with oxygen at different partial pressures. The resultant ionic defects may act as donors or acceptors contributing electrons to the conduction band or holes to the valence band thus leading to n or p-type semiconduction. The concentration of ionic defects, e.g., anion or cation vacancies, may also be compositionally controlled.

At relatively high temperatures, the assumption that thermodynamic equilibrium is established between the relative concentrations of ionic defects in the oxide crystal and the oxygen partial pressure in the gas phase appears to be valid. The interaction of electronic and ionic defects is therefore also governed by thermodynamic

considerations. Under these conditions, we may write equations relating the concentration of a particular defect species to oxygen partial pressure. By using the law of mass action we obtain a particular oxygen pressure dependence on concentration or electrical conductivity. The conductivity, σ_j, of a charge carrier species is related to its concentration by

$$\sigma_j = z_j e u_j c_j \tag{2-14}$$

where

z_j = electrochemical valence of species j
e = electronic charge
u_j = mobility
c_j = concentration

Because of interaction of various defect species, the presence of defects at high concentrations where activity coefficients are necessary, the formation of defect complexes and freezing in of defects below certain temperatures, it is usually difficult to separate unambiguously the various processes and associated energies of all species contributing to the electrical conductivity in Eq. (2-13).

The total conductivity at constant temperature may be expressed as a sum of terms of the type given in Eq. (2-14). When a conductivity-oxygen pressure dependence exists the total conductivity σ may be appropriately given by the expression

$$\sigma = K_{ion} P_{O_2}^{\pm 1/q'} + K_{\ominus} P_{O_2}^{-1/q''} + K_{\oplus} P_{O_2}^{+1/q'''} \tag{2-15}$$

where K_{ion}, $K_{\ominus}$, $K_{\oplus}$, and the q's are constants relating σ to P_{O_2} for ions, excess electrons $\ominus$, and electron defects $\oplus$. In oxide crystals where the number of oxygen ion vacancies is fixed by composition and is independent of temperature

and oxygen partial pressure, Eq. (2-15) simplifies to Eq. (2-14). The temperature dependence of ionic conductivity is then determined solely by the activation energy required for oxygen ion mobility. This situation appears to exist for zirconia-calcia solid solutions containing 0−45 mole % ceria in oxygen at 1 and 3.5×10^{-4} atm pressure. The conductivity data (Table 2-7) are therefore in agreement with the density data indicating that for fully oxidized ceria the number of oxygen ion vacancies remains constant (Section 2.3). Furthermore, our experimental results indicate that a Ce^{+4} ion size effect on oxygen ion mobility if present must be small (Section 2.4.2). We can therefore use these results to calculate the ionic and electronic conductivity components in mixed conduction where the oxygen ion vacancy concentration and thus the ionic conductivity has remained approximately constant.

In this type of defect structure, further oxygen vacancies, $\square$, may be formed by the loss of an equivalent amount of oxygen on normal lattice sites, $O^{=}$, to the gas phase, $O_2(g)$, according to the equation

$$O^{=} \rightleftharpoons \frac{1}{2} O_2(g) + \square + 2\ominus \qquad (2\text{-}16)$$

The oxygen vacancies act as donors and are able to contribute two electrons per vacancy to the conduction band. However, the Ce^{+4} ions present have an electron affinity such that the conduction electrons react with the Ce^{+4} lattice ions to form Ce^{+3} ions. The electron conduction is thus appreciably reduced.

The relative concentration of free conduction electrons depends on the relative energy levels of the conduction band and the Ce^{+4} acceptor levels. The overall reaction for the interaction of oxygen in the gas phase with the solid solution oxide crystal is

$$(2Ce^{+4} + O^{=})_{lattice} \rightleftharpoons \left(2Ce^{+3} + \square\right)_{lattice} + \frac{1}{2} O_2(g) \qquad (2\text{-}17)$$

The equilibrium constant, K_1, can be obtained by applying the law of mass action:

$$K_1 = P_{O_2}^{1/2} \frac{[\square]}{[O^{=}]} \frac{[Ce^{+3}]^2}{[Ce^{+4}]^2} \qquad (2\text{-}18)$$

The constant K_1 should be independent of composition at a particular temperature. Generally in defect crystals these thermodynamic relations have been found to hold for small defect concentrations.

Seven values of the thermodynamic constant K_1 for the reaction Eq. (2-18) are calculated from the microweighing data and presented in Table 2-16. The concentrations of the various species are in mole fractions and no corrections for differences in density are made. For a variation of oxygen pressure greater than 10^4, and for 6.5, 15, and 30 mole % ceria 5 values of K_1 are within a factor of 2 of each other for a disorder equilibrium where $\Delta C_{\square}$ (mole fraction) ≤ 0.06. For the other two samples $\Delta C_{\square} = 0.09$ and 0.11 and these K values are lower by a factor of 5 to 10 with respect to the other 5 values. (Average value of $K_1 = 42 \pm 22 \times 10^{-8}$.) The deviation for the 2 samples may be due to the large $\Delta C_{\square}$ values leading to formation of defect complexes and more tight bonding of lattice oxygen.

Another possibility is that sufficient time had not elapsed for equilibrium between the gas phase and the oxide to have been achieved and thus not all the oxygen was removed from the lattice.

Equation (2-18) should be applicable for reduction conditions where $Ce^{+3} \leq 0.2$. Equation (2-18) therefore breaks down for 100% ceria although the oxygen partial pressure dependence changes qualitatively in the right direction (Fig. 2-16).

Table 2-16

CALCULATED EQUILIBRIUM CONSTANT K_1 FOR EQ. (2-18) AT 1000°C

$-\log P_{O_2}$	$P_{O_2}^{1/2}$	$C_{\square} = 0.15 + \Delta C_{\square}$	$C_{O^=} = 1.85 - \Delta C_{O^=}$	$C_{\square}/C_{O^=}$	$\left[C_{C^{+3}}/C_{C^{+4}}\right]^2$	K_1
$C_{Ce^{+3}} + C_{Ce^{+4}} = 0.30$						
9.95	1.0×10^{-5}	0.205	1.80	0.114	0.335	3.8×10^{-7}
13.1	2.8×10^{-7}	0.239	1.76	0.136	2.19	8.4×10^{-8}
14.1	8.9×10^{-8}	0.255	1.74	0.150	5.27	7.0×10^{-8}
$C_{Ce^{+3}} + C_{Ce^{+4}} = 0.15$						
13.1	2.8×10^{-7}	0.209	1.79	0.168	12.6	6.0×10^{-7}
$C_{Ce^{+3}} + C_{Ce^{+4}} = 0.065$						
9.95	1.0×10^{-5}	0.163	1.84	0.089	0.39	3.5×10^{-7}
13.1	2.8×10^{-7}	0.177	1.82	0.097	24.1	6.5×10^{-7}
14.1	8.9×10^{-8}	0.180	1.82	0.099	96	8.5×10^{-7}

Brauer (Ref. 33) calculates a value of $\overline{\Delta H} = -180$ kcal/mole O_2 for the partial molar enthalpy of reaction of oxygen with $CeO_{1.83}$ solid solution at 850°C. From results of Table 2-12 for a 30 mole % ceria solid solution at $CeO_{1.83}$ a value of -133 kcal/mole O_2 was calculated between 1000 and 790°C from the equation

$$\overline{\Delta H} = RT_1T_2 \frac{\ell n\, P_2 - \ell n\, P_1}{T_2 - T_1} \tag{2-19}$$

where P is the equilibrium oxygen pressure at the particular temperature, and all other symbols have their usual meaning. The same $\overline{\Delta H}$ value was obtained for $CeO_{1.71}$ and $CeO_{1.65}$ (30 mole % ceria) and should remain constant throughout CeO_n. Reaction 2-17 is therefore endothermic with $\Delta H_1 = +133$ kcal/mole O_2 (+5.76 eV). As can be deduced from Eq. (2-19), the value of K_1 decreases or P_{O_2} over CeO_n decreases with decreasing temperature.

To obtain a term for the electronic conductivity component equivalent to the second term in Eq. (2-13) we proceed as follows: from Eq. (2-18) the ratio $C_{Ce^{+3}}/C_{Ce^{+4}}$ is given by

$$C_{Ce^{+3}}/C_{Ce^{+4}} = K_1^{1/2}\left(C_{O^{=}}/C_{\square}\right)^{1/2} P_{O_2}^{-1/4} \tag{2-20}$$

K_1, the equilibrium constant, is given by the standard thermodynamic expression

$$K_1 = \exp(\Delta S_1/kT) \exp(-\Delta H_1/kT) \tag{2-21}$$

where ΔS_1 is the standard entropy and ΔH_1 is the standard enthalpy [$\overline{\Delta H}$ in Eq. (2-19)] associated with Reaction (2-17). We may also write

$$K_1^{1/2} = A_1^{1/2} \exp(-\Delta H_1/2kT) \tag{2-22}$$

where the pre-exponential term $A_1 = \exp(\Delta S_1/k)$.

The conductivity-temperature data is expressed in terms of constant values of % CO in CO_2 $\left(\text{const. } P_{CO}/P_{CO_2}\right)$. It is therefore desirable to relate $P_{O_2}^{-1/4}$ Eq. (2-20) to P_{CO}/P_{CO_2}.

K_2 for the reaction

$$CO + \frac{1}{2}O_2 = CO_2 \tag{2-23}$$

is given by an expression equivalent to Eq. (2-22)

$$K_2^{1/2} = A_2^{1/2} \exp(-\Delta H_2/2kT) \tag{2-24}$$

so that from K_2 in reaction 2-23 and Eq. (2-24) we obtain

$$P_{O_2}^{-1/4} = \left(P_{CO}/P_{CO_2}\right)^{1/2} A_2^{1/2} \exp(-\Delta H_2/2kT) \tag{2-25}$$

The temperature dependence of oxygen partial pressure for several CO-CO_2 mixtures calculated from K values given by Darken and Gurry (Ref. 34) is shown in Fig. 2-17. From thermodynamic data (Ref. 36) $\Delta H_2 = -134.4$ kcal/mole O_2 (-5.82 eV) at 1200°K.

Substituting Eqs. (2-22) and (2-25) in Eq. (2-20) we obtain

$$C_{Ce^{+3}}/C_{Ce^{+4}} = A_1^{1/2} A_2^{1/2} \left(C_{O^{=}}/C_{\square}\right)^{1/2} \left(P_{CO_2}/P_{CO_2}\right)^{1/2} \exp\left[-(\Delta H_1 + \Delta H_2)/2kT\right] \tag{2-26}$$

For $C_{Ce^{+3}} \leq 0.2$ Eq. (2-26) simplifies to Eq. (2-27)

$$C_{Ce^{+3}}/C_{Ce^{+4}} = k'\left(P_{CO}/P_{CO_2}\right)^{1/2} \exp(-\Delta H'/2kT) \tag{2-27}$$

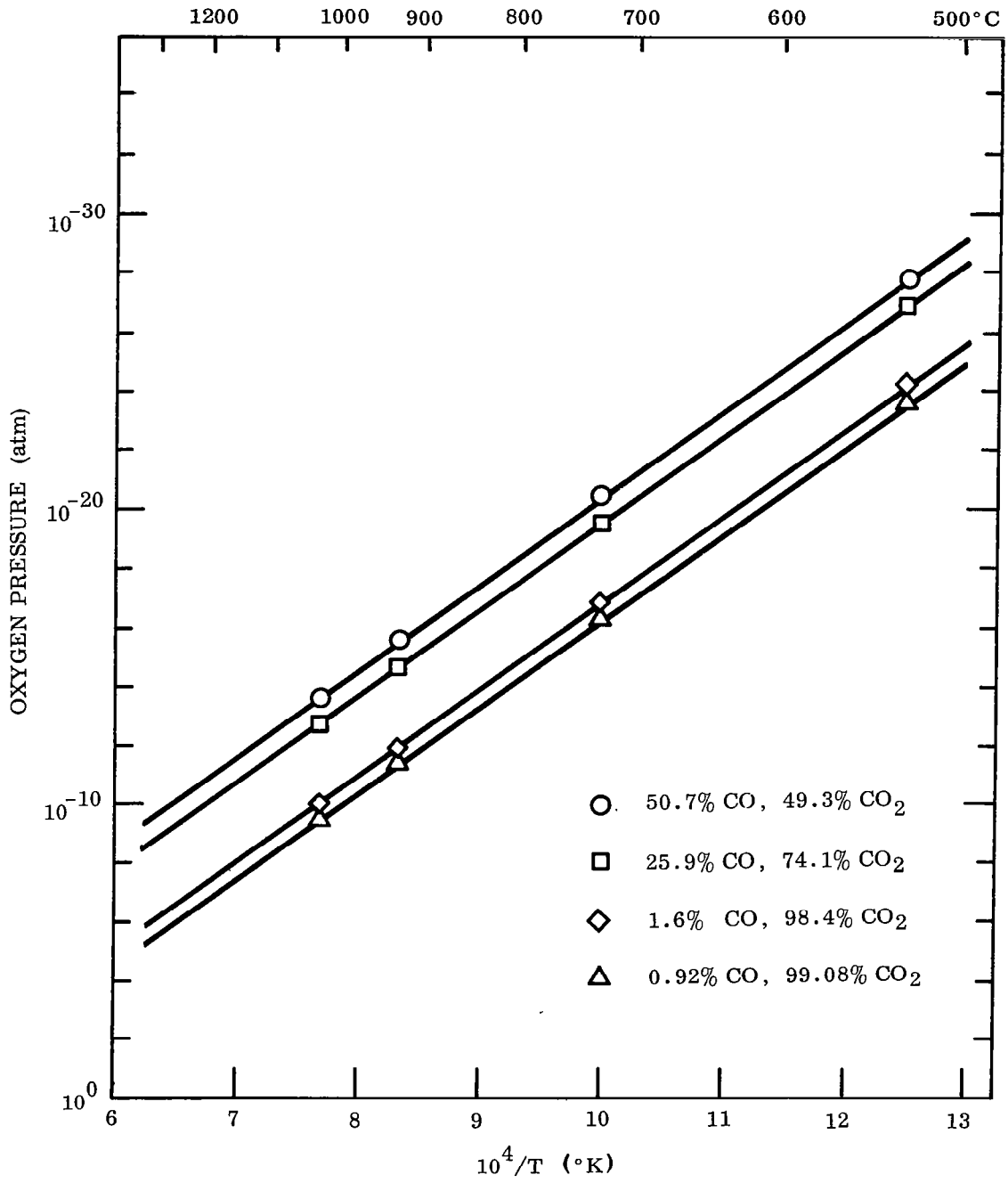

Fig. 2-17 Temperature Dependence of Oxygen Partial Pressure of Several $CO-CO_2$ Mixtures

where

$k' = A_1^{1/2} A_2^{1/2} \left(C_{O^=} / C_{\square} \right)^{1/2}$ since $\left(C_{O^=} / C_{\square} \right)^{1/2} \approx$ constant (Table 2-16) and

$$\Delta H' = \Delta H_1 + \Delta H_2 \qquad (2\text{-}28)$$

Since

$$\Delta H_1 + \Delta H_2 = \Delta H' \approx 0 \qquad (\text{for } x = 0.30)$$

the $C_{Ce^{+3}}/C_{Ce^{+4}}$ ratio or $C_{Ce^{+3}}$ (for constant x) should be very nearly independent of temperature and remain approximately constant at constant % CO in CO_2. This is verified experimentally.

A statistical distribution of Ce^{+4} and Ce^{+3} ions in reduced $(ZrO_2)_{0.85-x}(CeO_2)_x (CaO)_{0.15}$ is expected to occur in the cation lattice. Very nearly all of the electrons released from Reaction (2-16) are trapped by Ce^{+3} ions. Ce^{+3} ions can exchange electrons with adjacent Ce^{+4} leading to a hopping mechanism of electron conduction. Zr^{+4} and Ca^{+2} ions are blocking to electron transfer or exchange. The number of continuous paths which exist for electron transfer through the crystal is therefore proportional to x, the mole fraction of ceria (Ce^{+4} + Ce^{+3}). For a constant x an activation energy Q_3 may be associated with the Ce^{+3} - Ce^{+4} electron hopping mechanism and should be independent, at least to a first approximation, of $C_{Ce^{+3}}$. Experimentally the total activation energy for electronic conduction was found to be approximately independent of $C_{Ce^{+3}}$ for constant x (Fig. 2-10). As a function of x the total activation energy decreases rapidly at low x, approaches a constant value asymptotically, and is approximately constant at $x \geq 0.15$ (Fig. 2-10).

For constant x the electronic conductivity should therefore be proportional to mole fraction $C_{Ce^{+3}}$ and to a term $A_3 \exp(-Q_3/kT)$.

To solve for $C_{Ce^{+3}}$ at any mole fraction ≤ 0.2 we proceed as follows: From $C_{Ce^{+3}}/C_{Ce^{+4}} = B$ defined by Eq. (2-27) and

$$C_{Ce^{+3}} + C_{Ce^{+4}} = x \tag{2-29}$$

we obtain

$$C_{Ce^{+3}} = xB/(1 + B) \tag{2-30}$$

Therefore for a constant value of x (x = c) and assuming $\Delta H' \approx 0$ for all values $0 < x < 0.30$

$$\sigma_e = \frac{ck'\left(P_{CO}/P_{CO_2}\right)^{1/2}k''}{1 + k'\left(P_{CO}/P_{CO_2}\right)^{1/2}} \exp\left(-Q_3/kT\right) \tag{2-31}$$

where k'' is a constant relating σ_e to $C_{Ce^{+3}}$. From Eq. (2-31) a plot of log σ vs. 1/T at constant %CO in CO_2 gives Q_3. At a constant temperature and for x and σ_i constant, the electronic conductivity σ_e is 0 at $Ce^{+3} = 0$ and should be proportional to $C_{Ce^{+3}}$ or to $(P_{CO}/P_{CO_2})^{1/2}$ for $k'(P_{CO}/P_{CO_2})^{1/2} << 1$. According to Eq. (2-25), $(P_{CO}/P_{CO_2})^{1/2} = kP_{O_2}^{-1/4}$ at constant temperature.

Conductivity as a function of P_{O_2} for 15 mole % ceria at three constant temperatures is shown in Fig. 2-11. At 560 and 727 °C an increase of σ with decrease of P_{O_2} is clearly noted. (At 977 °C the conductivity is predominately ionic.)

The conductivity curve for 727 °C is replotted in Fig. 2-18 in terms of conductivity as a function of $C_\square$, the mole % oxygen vacancies and $C_{Ce^{+3}}$. The rise in conductivity occurs in the 15 to 16 mole % $C_\square$ interval. The mole fraction of $C_{Ce^{+3}}$ therefore increases from 0 to 0.02. The conductivity remains approximately constant with a doubling of $C_{Ce^{+3}}$ to 0.04 and then decreases with further increase in concentration

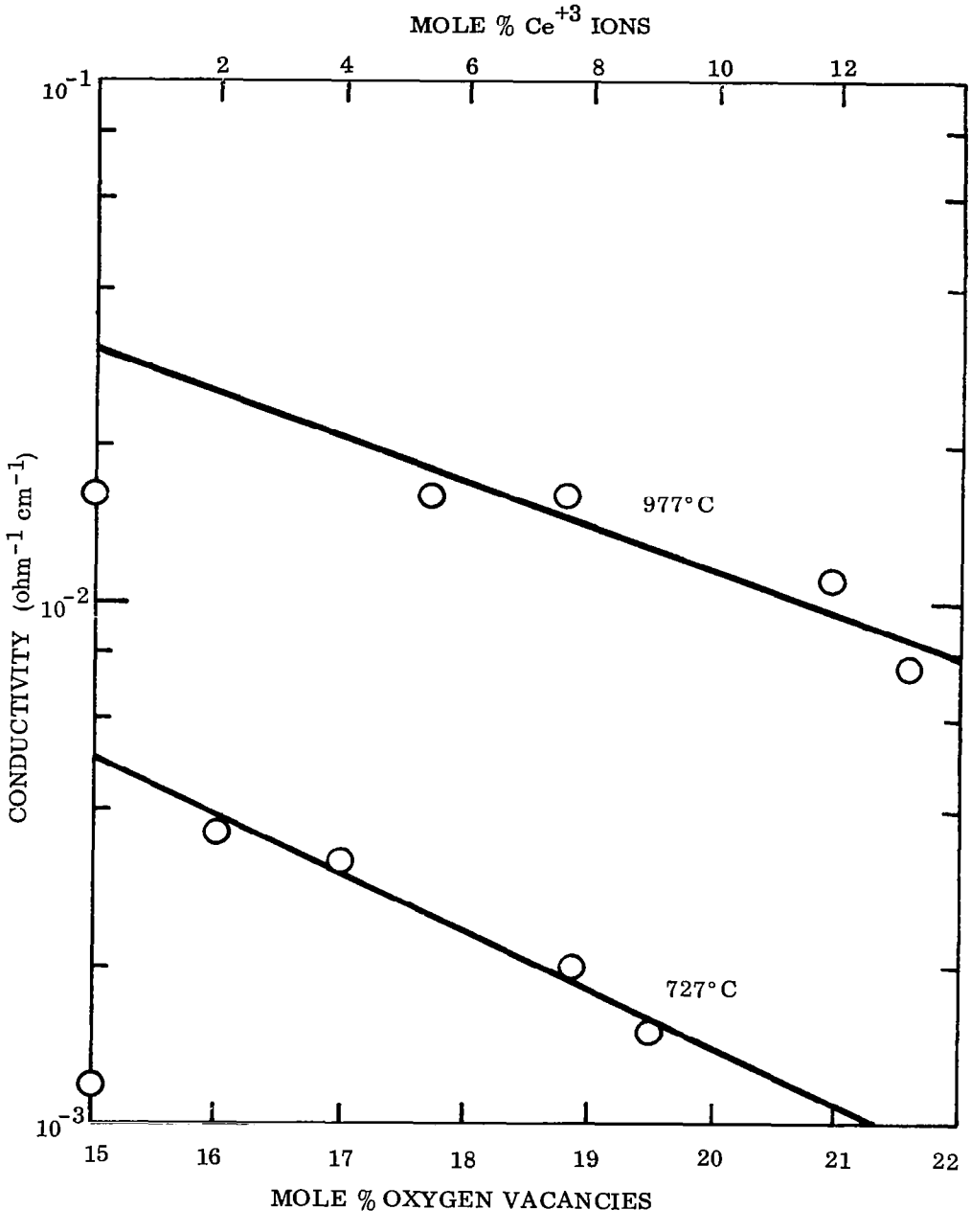

Fig. 2-18 Dependence of Conductivity on Mole Percent Oxygen Vanancies and Ce^{+3} Ions in $(ZrO_2)_{0.70}(CeO_2)_{0.15}(CaO)_{0.15}$ at 727° and 977° C

of Ce^{+3}. A sufficient number of points over a large σ and P_{O_2} interval is not available to obtain a very precise value of the slope. From the slope found in Fig. 2-11 a value of 7 was calculated for q in $P_{O_2}^{-1/q}$ at 727 °C. (The theoretical value is 4.)

Figure 2-12 shows a plot of conductivity vs. mole % ceria at four different temperatures for 1.6% CO in CO_2. The electronic conductivity increases approximately linearly with increasing mole % ceria at low mole % ceria but appears to be leveling off and approaching a constant value of σ at higher values of ceria. The electronic conductivity appears to be at a maximum near 1.6% CO in CO_2 and a further increase in $C_{Ce^{+3}}$ does not increase conductivity but has the opposite effect (Fig. 2-18).

As a first approximation, from Fig. 2-12 the number of Ce^{+3}-Ce^{+4} conducting paths through the crystal can be taken as varying in a linear manner in the region 0−30 mole %. Therefore in the range 0−30 mole % the electronic conductivity should to be proportional to x the total ceria concentration, and to Ce^{+3}. From this picture for a constant value of $x, 0 < x < 0.30$, it appears reasonable that the σ_e should reach a maximum and level off with increasing Ce^{+3}. A drop in conductivity is more difficult to explain. The total conductivity is measured as a sum an electronic and ionic component.

The following explanation may be proposed for a drop in the electronic component of conductivity: when ceria in the solid solution approaches the fully reduced state (depending on the total ceria concentration or the total number ceria paths through the electrolyte) electronic conduction by Ce^{+4}-Ce^{+3} electron hopping is replaced by a different mechanism. In solutions with ceria ≤ 15 mole % this leads to a large drop in electronic conductivity from its peak value but in solutions with 30 mole % ceria a similar large drop in the conductivity is not evident (Fig. 2-9). The change in the value of the activation energy with composition (Fig. 2-10) may be associated with this effect.

With increasing reduction of Ce^{+4} to Ce^{+3} the concentration of oxygen vacancies is no longer constant but increases appreciably (Fig. 2-18). For zirconia-calcia solid solution evidence is available in the literature (Refs. 17, 20, 21) that the ionic conductivity goes through a maximum and then decreases with increasing oxygen vacancy concentration. Tien and Subbarao (Ref. 18) did not find a conductivity maximum but in the range 13−20 mole % oxygen vacancies the log of the conductivity was found to decrease at an approximately linear rate. At 977 °C for 15 mole % ceria the total conductivity is

predominately ionic (Fig. 2-18) and a decrease of conductivity with increasing oxygen vacancy concentration is evident. It may be that we are in a region where a maximum in ionic conductivity exists, falling off sharply with increasing oxygen vacancy concentration or possibly with increasing Ce^{+3} ion concentration due to an ion size effect decreasing the oxygen ion mobility. Another possible explanation may involve an ordering of the fluorite structure at large Ce^{+3} concentrations in this particular temperature range leading to a decrease in the ionic conductivity component. At lower temperatures, this decrease in ionic conductivity may account only for a fraction of the total decrease in conductivity (727 and 560 °C).

The fraction of ion and electron component contributing to the electronic conductance may be calculated from the conductivity-temperature data and the equations presented for a very wide range of conditions. Transport number data from EMF measurements and oxygen efficiency data on cells containing these mixed oxides as electrolytes should help in further interpreting the conductivity behavior of this oxide system.

Section 3

ELECTROLYSIS OF CO_2-H_2O MIXTURES

3.1 ZIRCONIA-CALCIA TUBE CELLS

Mixtures of carbon dioxide and water vapor were electrolyzed at temperatures less than 800°C using the tube cell apparatus shown in Figs. 3-1 and 3-2. A tube of composition $(ZrO_2)_{0.85}$ $(CaO)_{0.15}$ 1 mm thick with porous platinum electrodes each 1 cm^2 in area served as the electrolytic cell. The output of each reaction product, oxygen, carbon monoxide, and hydrogen was monitored to determine the distribution of the current between CO_2 and H_2O electrolysis as well as the total current efficiency (i.e., the oxygen current efficiency). The CO_2 flow rates were relatively high compared to the current to prevent concentration polarization, and no more than 8% of the available CO_2 was reduced in any run.

3.1.1 Experimental Results

The experimental data are summarized in Table 3-1. Since the electrode area was 1 cm^2, values of the current and current density are the same. The gas flow pattern is illustrated schematically in Fig. 3-3. The carbon dioxide flow rate, j'_{CO_2}; oxygen flow rate, j_{O_2}; gas outflow, j_{OUT}; electrolysis current, i; and water saturater temperature, t, were read directly. All of the other flow rates were calculated from these data and the gas analysis data using the following relationships:

$$j'_{CO_2} = j_{CO} + j_{CO_2} \tag{3-1}$$

$$j_{OUT} = j_{CO_2} + j_{CO} + j_{H_2} = j'_{CO_2} + j_{H_2} \tag{3-2}$$

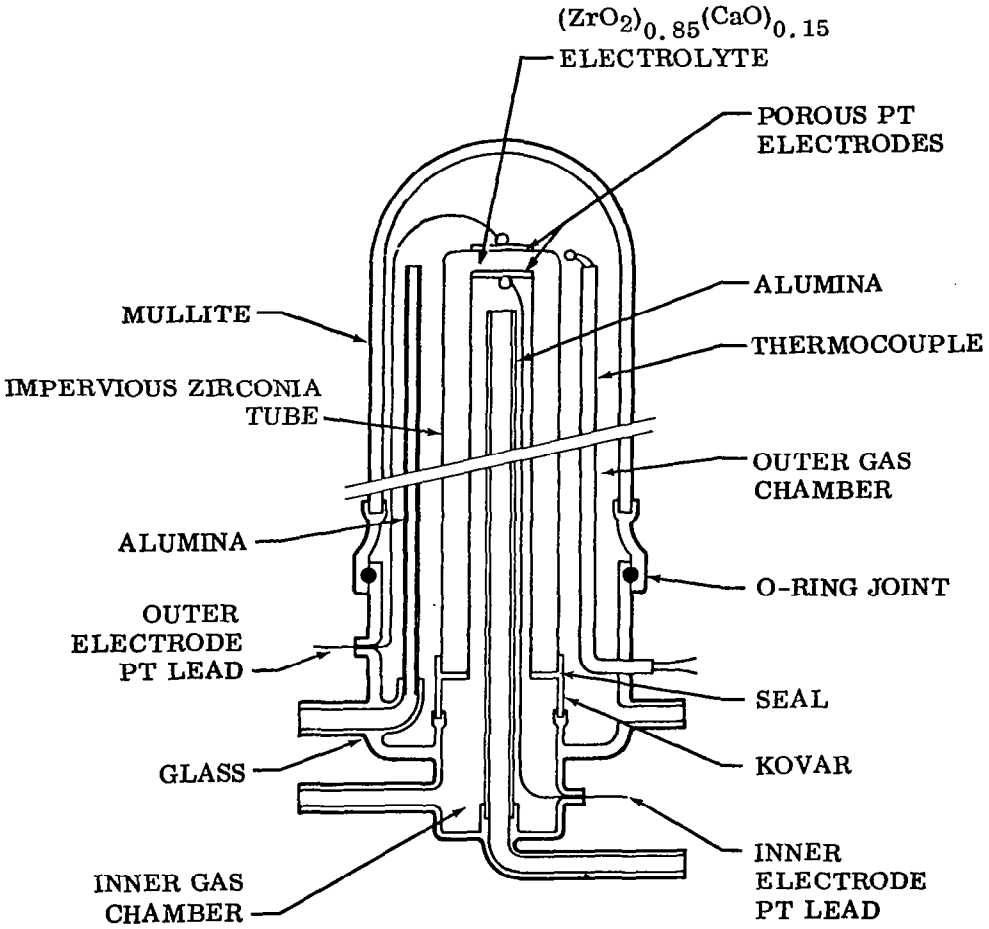

Fig. 3-1 Tube Cell

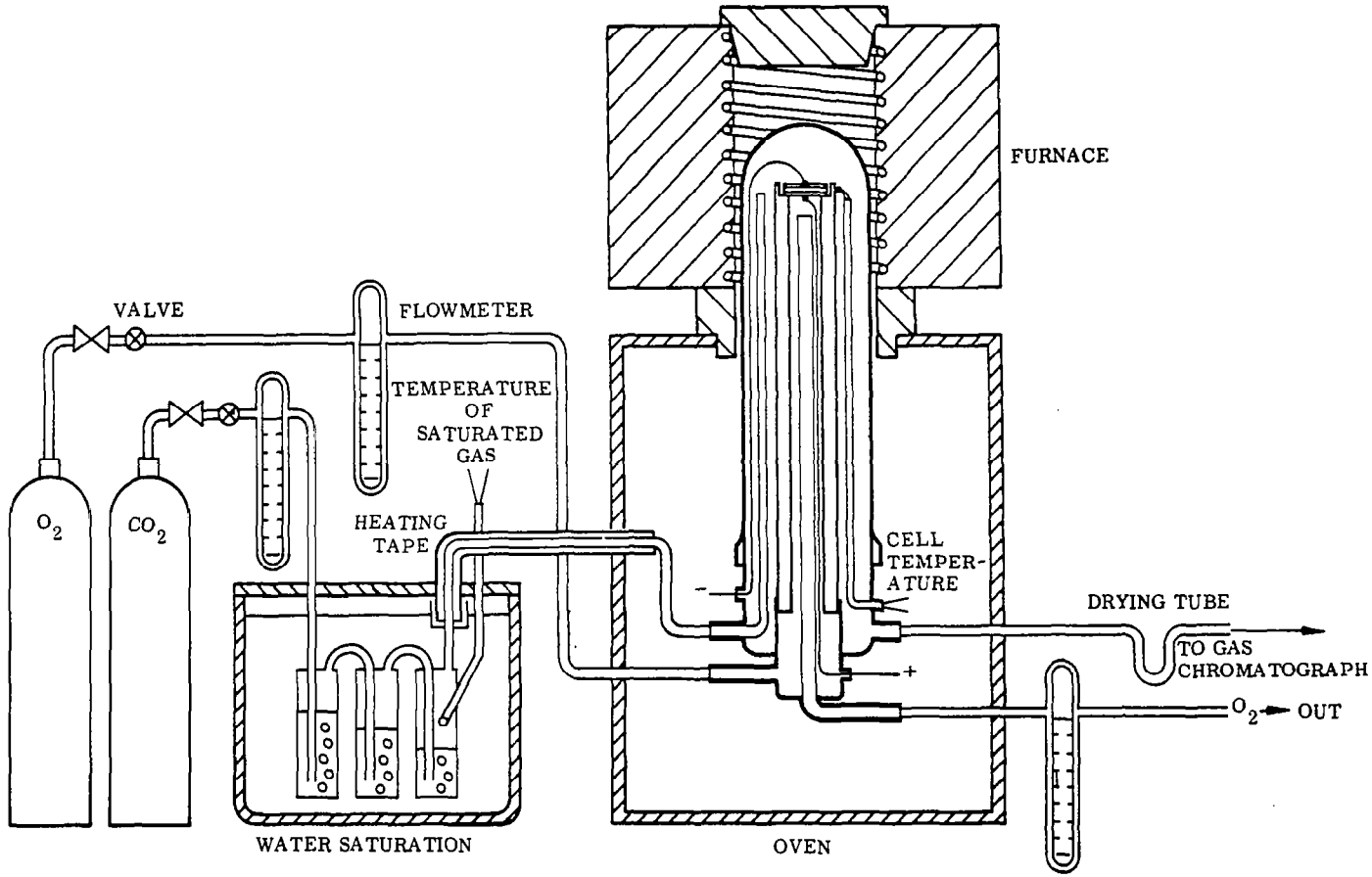

Fig. 3-2 CO_2-H_2O Electrolysis System

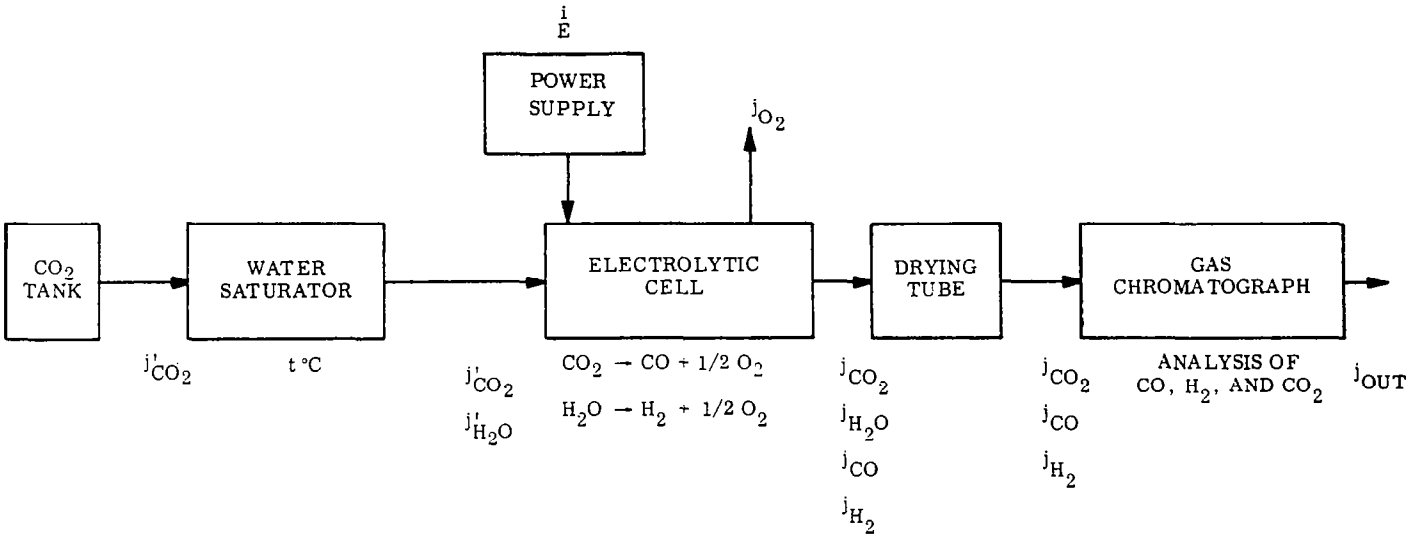

Fig. 3-3 Flow Diagram

Table 3-1

SUMMARY OF ELECTROLYSIS RUNS

Run	t (°C)	i (mA)	E (volts)	j'_{CO_2} (ml/min)	j'_{H_2O} (ml/min)	j_{CO} (ml/min)	j_{H_2} (ml/min)	C.E.$_{(O_2)}$ (%)	O_2 Yield (ml/min/watt)
1	730.2	50	6.22	12.85	2.36	0.047	0.27	89	0.55
2	784.3	50	4.13	6.21	0.23	0.26	0.11	100	0.93
3	791.3	50	2.68	4.95	0	0.052	0	19	0.27
4	735.7	100	7.95	12.29	0.45	0.24	0.25	63	0.30
5	735.4	100	8.68	12.67	2.38	0.13	0.46	79	0.34
6	735.5	100	8.38	12.91	2.44	0.10	0.45	74	0.33
7	734.8	100	8.33	5.75	1.06	0.14	0.40	68	0.31
8	731.7	100	7.83	6.21	0.22	0.29	0.19	63	0.31
9	788.0	100	5.62	6.29	0.23	0.41	0.19	76	0.51
10	793.2	100	3.34	5.66	0	0.10	0	15	0.18
11	783.4	150	5.42	6.31	0.23	0.40	0.19	50	0.34

NOTE: 100% current efficiency is equivalent to 0.76 ml/min of CO_2, H_2O, CO, or H_2 at 100 mA and to 0.38 ml/min of O_2 at 100 mA (1 atm, 25° C)

$$j_{H_2} = \frac{\text{fraction } H_2}{1 - \text{fraction } H_2} j'_{CO_2} = \text{fraction } H_2 \times j_{OUT} \quad (3\text{-}3)$$

$$j_{CO} = \text{fraction CO } (j'_{CO_2} + j_{H_2}) = \text{fraction CO} \times j_{OUT} \quad (3\text{-}4)$$

$$j'_{H_2O} = \frac{P_{H_2O}}{P_{CO_2}} j'_{CO_2} \quad (3\text{-}5)$$

Note: fraction H_2 and fraction CO are from the gas analysis

Current efficiencies were calculated from the oxygen output and also from the hydrogen and carbon monoxide outputs. It will be seen that more measurements than necessary were taken so that the self-consistency of the data could be checked. The values reported here are believed to be within ± 3%.

The catalytic effect of water vapor on the electroreduction of CO_2 is shown in Table 3-2.

Table 3-2

CATALYTIC EFFECT OF WATER VAPOR

Run	~t (°C)	i (mA)	j'_{H_2O} (ml/min)	C.E. (O_2) (%)	C.E. (CO) (%)	O_2 Yield $(\frac{ml/min}{watt})$
3	785	50	0	19	19	0.27
2	785	50	0.23	100	70	0.93
10	790	100	0	15	15	0.18
9	790	100	0.23	76	54	0.51
8	733	100	0.22	63	38	0.31
7	733	100	1.66	68	18	0.31

As the table illustrates, at the temperature of these runs (~790° C) the addition of water vapor improved the current efficiency for the reduction of CO_2 to such an extent that it would be beneficial to add water even if the product hydrogen were lost

and did not subsequently attain equilibrium according to the water shift reaction,

$$CO_2 + H_2 \rightleftharpoons CO + H_2O \qquad (3\text{-}6)$$

Tables 3-1 and 3-2 also show that only small additions of H_2O vapor to the CO_2 stream are needed (equivalent to equilibrium water-water vapor saturation at room temperature for run 8) to obtain a significant improvement in efficiency. A further increase in j'_{H_2O} by a factor of 5 increases the efficiency only moderately. (See also runs 4, 5, and 6.)

The strong influence of current density on the current efficiency for electrolysis at approximately 785 °C of a CO_2-H_2O mixture is shown in Table 3-3. At a current density of 100 mA/cm^2, the electrolyte was 76% ionically conducting, and if the water shift reaction were to reach equilibrium at the cell operating temperature, almost all of the ionic current would go to produce CO.

Table 3-3

CURRENT EFFICIENCY VS. CURRENT DENSITY

Run	i (mA/cm^2)	C. E.$_{(O_2)}$ (%)	C. E.$_{(CO)}$ (%)	C. E.$_{(CO)}$ at Equil. (calculated)
2	50	100	70	97
9	100	76	54	76
11	150	50	34	50

3.1.2 Water Shift Equilibrium

Attainment of the water shift equilibrium, (3-6), would significantly improve the net current efficiency for CO_2 reduction since the equilibrium constant at the temperatures of these experimental runs lies between 0.7 and 0.9 (Ref. 34). Figure 3-4 shows the calculated current efficiency for CO_2 reduction as a function of water vapor flow rate for three cases:

(a) The water shift reaction is at equilibrium

(b) All of the water vapor is reduced before CO_2 reduction occurs

(c) The distribution of current is the same as the relative proportions of CO_2 and H_2O in the inlet gas stream

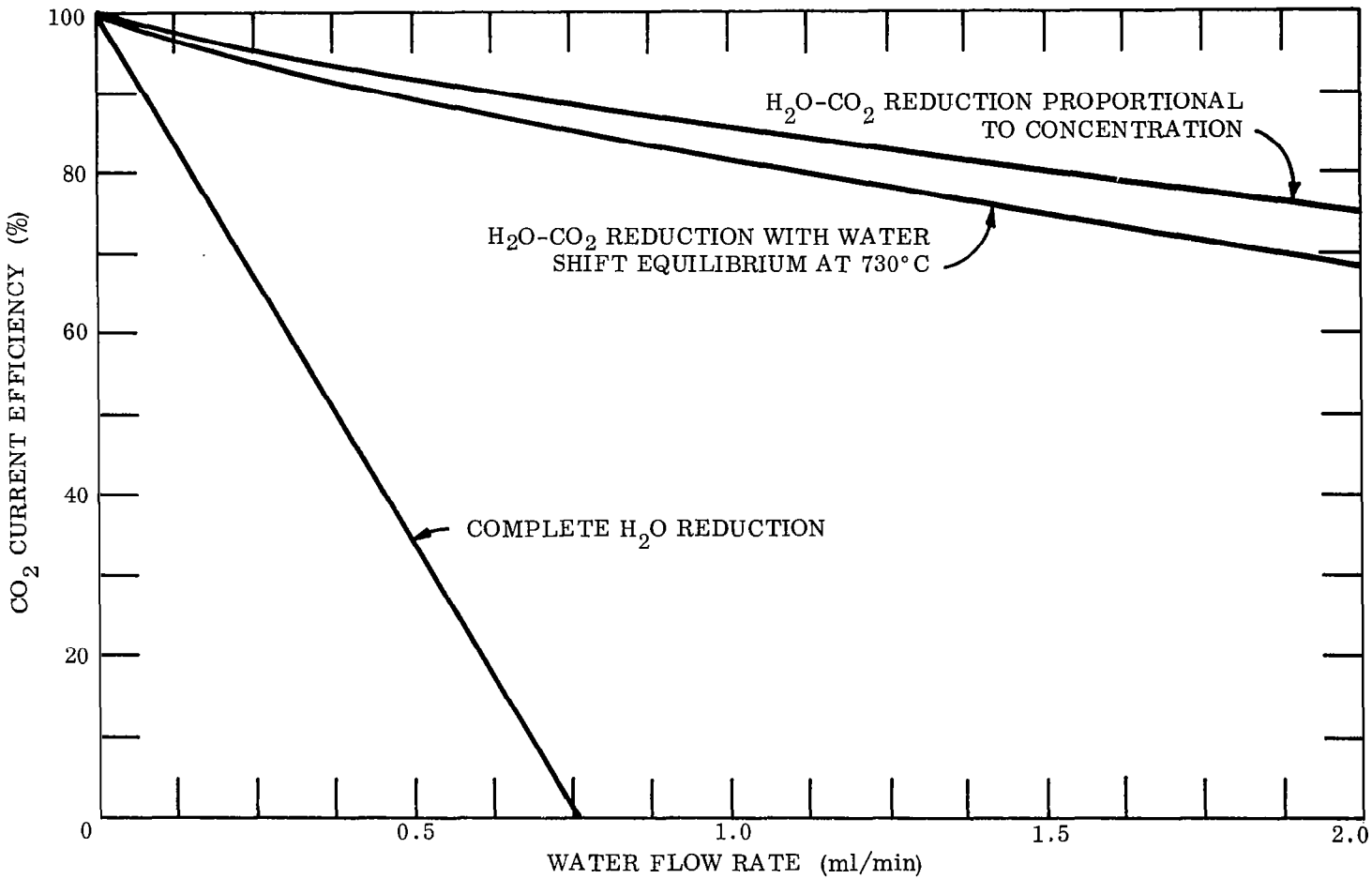

Fig. 3-4 Calculated CO_2 Current Efficiency on Electrolysis of H_2O-CO_2 Mixtures at 730°C, 100% Total Current Efficiency, 100 mA Current, CO_2 Flow 6.0 ml/min

The equilibrium line on Fig. 3-4 was calculated for the arbitrary conditions stated in the figure. A similar calculation of the equilibrium point for the actual conditions in each run follows.

In the electrolytic system, the following relationships hold:

$$j_{H_2O} = j'_{H_2O} - j_{H_2} \tag{3-7}$$

$$j_{CO_2} = j'_{CO_2} - j_{CO} \tag{3-8}$$

At equilibrium, the equilibrium condition also applies:

$$\frac{P_{CO}P_{H_2O}}{P_{CO_2}P_{H_2}} = K(t) = \frac{j_{CO}j_{H_2O}}{j_{CO_2}j_{H_2}} \tag{3-9}$$

Substituting for j_{H_2O}, j_{CO_2}, and j_{H_2} gives

$$\frac{j_{CO}(j'_{H_2O} - j_{H_2})}{(j'_{CO_2} - j_{CO})\,[(j_{H_2} + j_{CO}) - j_{CO}]} = K(t) \tag{3-10}$$

Since the current was sufficient to convert only a fraction of the CO_2 and since the equilibrium constant was close to unity,

$$j_{H_2} < j'_{H_2O} \quad \text{and} \quad j_{CO} < j'_{CO_2} \tag{3-11}$$

Thus,

$$j_{CO} \approx \frac{Kj'_{CO_2}(j_{H_2} + j_{CO})}{Kj'_{CO_2} + j'_{H_2O}} \tag{3-12}$$

Values of j_{CO} and j_{H_2} calculated from this approximation for each run are shown in Table 3-4. The K's are those of Darken and Gurry (Ref. 34).

In the runs in Table 3-1 at 730−800 °C, it is apparent that a large fraction (0.32 to 0.84) of the total oxygen evolved electrolytically at the anode is obtained from the water in the CO_2 stream but in no case is the water reduced in accordance with the calculated line (complete H_2O reduction) in Fig. 3-4. Since an appreciable fraction of the gas stream flowing through the cathode chamber does not come in contact with the electrode a separate catalytic reactor may not be needed if the multiple cell and gas flow system were properly designed or if Ni, Fe, or Ni-Pt or Fe-Pt alloy cathodes were used.

Table 3-4

COMPARISON OF EXPERIMENTAL AND EQUILIBRIUM CONDITIONS

Run	t (°C)	Experimental				Equilibrium		
		K	j_{CO} (ml/min)	j_{H_2} (ml/min)	C.E.$_{(O_2)}$ (%)	j_{CO} (ml/min)	j_{H_2} (ml/min)	C.E.$_{(CO)}$ (%)
1	730.2	0.72	0.047	0.27	89	0.25	0.067	66
2	784.3	0.90	0.26	0.11	100	0.37	0.00	97
3	791.3	0.90	0.052	0	19	0.052	(No H_2O)	14
4	735.7	0.73	0.24	0.25	63	0.47	0.02	62
5	735.4	0.73	0.13	0.46	79	0.47	0.12	62
6	735.5	0.73	0.10	0.45	74	0.44	0.11	58
7	734.8	0.73	0.14	0.40	68	0.43	0.11	57
8	731.7	0.72	0.29	0.19	63	0.46	0.02	61
9	786.7	0.90	0.41	0.19	76	0.58	0.02	76
10	793.2	0.90	0.10	0	15	0.10	(No H_2O)	13
11	783.4	0.90	0.40	0.19	50	0.57	0.02	50

3.2 ZIRCONIA-CALCIA-CERIA DISK CELLS

The small disk is a convenient geometry for the fabrication and characterization of solid oxide electrolytes. For conducting electrolysis experiments with electrolyte disks, an apparatus was built to enable the two sides of the disk to be separated by gas-tight high-temperature seals such that quantitative measurements could be made of the changes taking place at the cathode, the anode, and inside the electrolyte. This approach permits solid electrolytes of various compositions not available commercially to be studied under conditions of electrolysis of gases without having to fabricate high-fired ceramic bodies with complicated shapes.

3.2.1 Apparatus

The disk electrolysis apparatus is shown schematically in Fig. 3-5. The electrolyte disk, held between two ceramic tubes having flat ends, is attached to each tube by

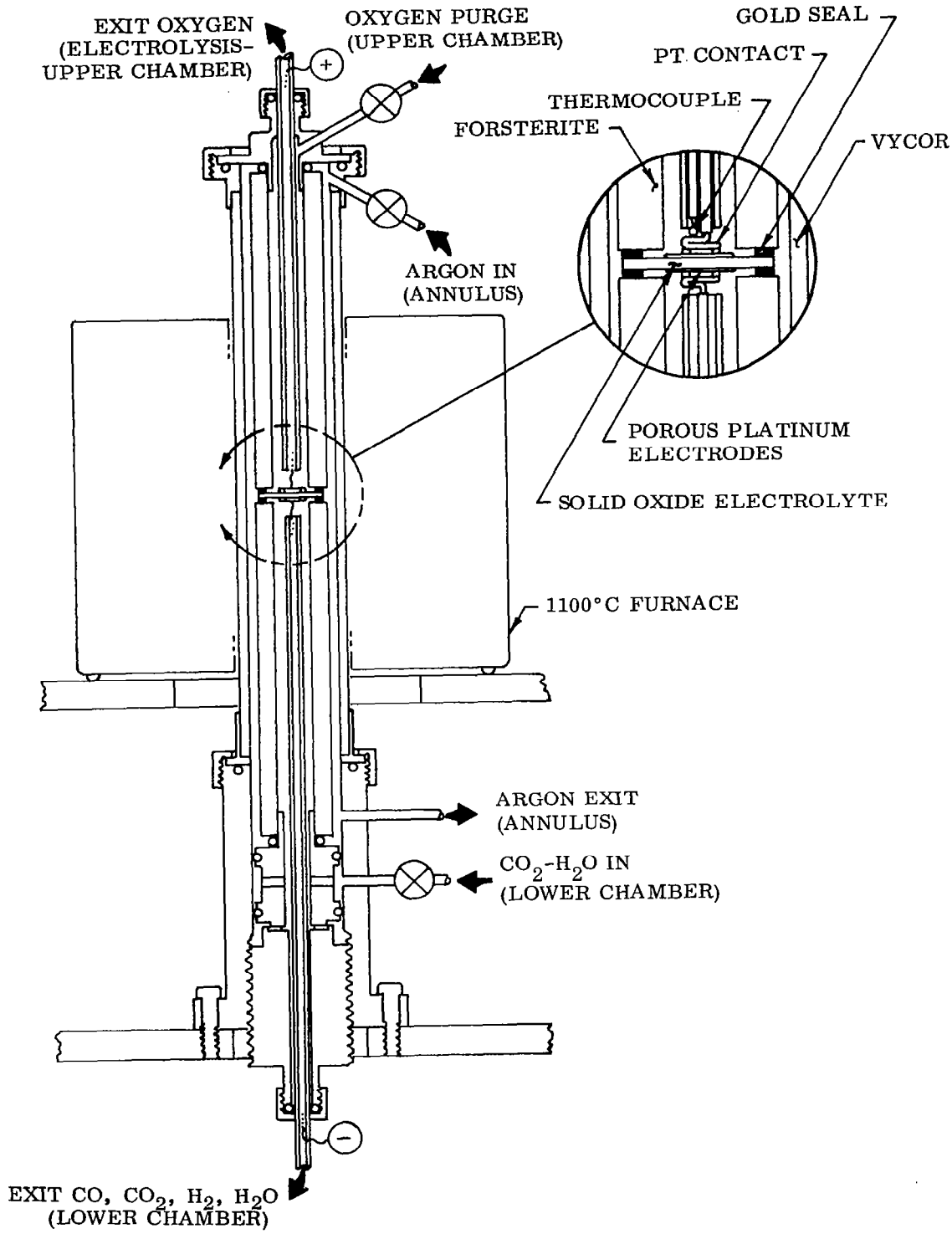

Fig. 3-5 Sealed Disk Electrolyte Test Unit

a gas-tight high-temperature seal. The seals are formed by a combination of the high temperature provided by a split furnace enclosing the assembly and mechanical pressure applied by the screw underneath the lower tube. An outer quartz tube holds the upper tube in alignment and also enables the atmosphere to be controlled. Once gas-tight seals have been formed, the apparatus has three separate gas compartments, the upper and lower chambers (i.e., cathode and anode sides), and the annulus. Each compartment is provided with a gas inlet and outlet to permit different gases to flow through independently. A thermocouple is located in the upper chamber close to the electrolyte disk. The temperature can be varied from ambient to 1100°C.

3.2.2 High-Temperature Seals

Several sealing techniques were tried that did not give satisfactory performance. These will be described briefly and the reasons for their failure will be discussed. The prime criteria for useful seals are gas-tightness, freedom from interference with the electrodes, lack of spurious electrochemical effects, and ease of forming and demounting.

A glass seal using O. Hommel Vitreous Enamel 38 (O. Hommel Co., Los Angeles) gave a gas-tight seal but the glass flowed over the electrodes, thereby interfering with electrolysis. Furthermore, at the operating temperature of the cell, the glass was electrically conducting; such conductivity could cause short-circuiting of the cell.

A seal was attempted by melting a gold washer between the platinized electrolyte disk and the ceramic tube. This method failed completely because the molten gold did not wet the tube, but instead formed little balls.

The surface was rendered wettable to molten gold by applying a thin platinum paste film to the ceramic before assembling the cell. With this arrangement, the molten gold alloyed with the platinum and formed a gas-tight seal. However, with air/O_2, the correct electromotive force was not found, nor was 100% current efficiency obtained on operating the cell as an oxygen-transfer cell. It seems likely that parasitic electrolytic cells were formed at the edges of the disk resulting in electrochemical oxygen transfer into the annulus and electrical interference with the cell electrodes.

A seal was attempted by relying on heat and pressure to alloy a gold washer to a platinized area on the disk not connected to the platinized electrode. The seal thus formed leaked up to the highest temperature of the run, 992°C.

The seal formed by compressing a thin gold washer between an unplatinized area of the electrolyte disk and the flat end of the ceramic (Forsterite, American Lava Corp., Chattanooga, Tenn.) tube at high temperature has met our sealing criteria. Gas-tightness was checked by applying pressure to one chamber of the apparatus and monitoring any flow from the other chambers as well as by measuring the open-circuit cell potential for air/oxygen and for $CO\text{-}CO_2/O_2$ with a 15 mole % calcia-zirconia electrolyte. The electrodes consisted of platinized areas on each side of the disk not in electrical contact with the gold washers to minimize possible spurious electrical effects involving the seals. Seals formed in this way gave no detectable electrochemical oxygen transfer at the edges of the electrolyte disk. All of the electrolysis results presented in this section were obtained with disks having gold compression seals of this type.

The thermal expansion coefficients of the materials involved are Forsterite-110, gold-140, calcia-stabilized zirconia-100×10^{-7} cm/cm-°C. The seals remained unbroken by differential contraction upon cooling to room temperature. After removing the two Forsterite tubes with seals and disk intact, the two chambers were leak-checked separately and found to be gas-tight and the assembly was then broken apart by use of sufficient force. The rupture occurred primarily through the disk rather than at the gold seal. Visual examination of the seal revealed that the gold washer had formed a good bond with both the Forsterite and the electrolyte around its entire periphery.

During electrolysis, mechanical pressure was maintained on the seal with the screw. The behavior of the seal at high temperature with mechanical pressure relieved has not yet been investigated. This sealing technique seems to be satisfactory for electrolytic studies with laboratory-scale electrolyte disks where conditions can be monitored continuously, but an extrapolation to a larger unit would appear to require further work.

3.2.3 Results and Discussion

Electrolysis runs were made with electrolytes of two compositions: $(ZrO_2)_{0.85}(CaO)_{0.15}$ and $(ZrO_2)_{0.82}(CaO)_{0.15}(CeO_2)_{0.03}$. Air, oxygen, CO_2-H_2O, and CO-CO_2 were electrolyzed in the temperature range, 840 to 1007°C. The runs are tabulated chronologically in Tables 3-5 and 3-6. The symbols are the same as those used in Section 3-1. One electrolyte disk was used for the seven runs in Table 3-5, four different disks provided the data in Table 3-6. Voltages shown are corrected for IR drop in the lead wires, but no corrections have been made for the differences in disk thickness (from 1.3 to 2.0 mm). For this reason, and because of imperfect contacts to the electrodes, the oxygen energy yield column must be regarded as indicative rather than exact. The precision of the other measurements is estimated as ±2%.

The extent of variability of cell performance from run to run can be gauged from Table 3-7. The large differences in oxygen energy yield shown there in several instances probably result mainly from poor electrode contacts with the need for a higher applied voltage, but an aging effect might also have been a contributing cause.

The cell voltage, in principle, will consist of the following terms:

$$E_A = E_N + E_p + E_c + I(R_o + R_c + R_L) \qquad (3\text{-}13)$$

where

E_A = applied voltage

E_N = reversible, or Nernst, voltage

E_p = activation polarization

E_c = concentration polarization

I = current

R_o = oxide resistance

R_c = contact resistance

R_L = lead resistance

Table 3-5

ELECTROLYSIS RUNS IN CHRONOLOGICAL ORDER
$(ZrO_2)_{0.85}(CaO)_{0.15}$

Electrode area = 0.71 cm^2
Thickness = 1.4 mm

Run	Note-book page	t (° C)	i (mA)	i/A (mA/cm^2)	E (V)	E Corrected for IR in leads	j'_{CO_2} (ml/min)	j'_{H_2O} (ml/min)	j_{O_2} (ml/min)	C.E.$_{(O_2)}$ (%)	O_2 Yield $\frac{ml/min}{watt}$
1	38	969	50	70			(a)	(a)	0.190	100	
2	42	982	50	70	1.08-1.86 (b)	1.03-1.81 (b)	6.0	0.15	0.184	96.8	2.03
3	42	982	75	105	2.22	2.15	8.8	0.22	0.285	100	1.77
4	42	982	100	140	2.68	2.58	8.8	0.22	0.378	99.5	1.46
5	42	986	150	210	3.64	3.49	8.8	0.22	0.576	101	1.10
6	42	841	50	70	4.64	4.59	8.8	0.22	0.190	100	0.83
7	42	841	75	105	6.09	6.02	8.8	0.22	0.211	74.1	0.47

(a) Oxygen electrolysis, j'_{O_2} = 5.0 ml/min.

(b) The initial voltage was 1.08 V but it increased to 1.86 V upon continued electrolysis. The CO_2-H_2O side of the cell might not have been thoroughly purged of oxygen at the start of electrolysis.

Table 3-6

ELECTROLYSIS RUNS IN CHRONOLOGICAL ORDER $(ZrO_2)_{0.82}(CaO)_{0.15}(CeO_2)_{0.03}$

Run	Note-book page	t (° C)	i (mA)	i/A (mA/cm^2)	E (V)	E Corrected for IR in leads	j'_{CO_2} (ml/min)	j'_{H_2O} (ml/min)	j_{O_2} (ml/min)	C. E.$_{(O_2)}$ (%)	O_2 Yield $\frac{ml/min}{watt}$
8[a]	44	986	51	68	0.82	0.77	(b)	(b)	0.194	100	4.95
9	44	986	150	200	2.18	2.03	(b)	(b)	0.585	102	1.92
10	46	986	50	67	0.91	0.86	6.0	0.16	0.157	82.6	3.65
11[d]	48	1004	100	140	0.99	0.89	(c)	(c)	0.378	99.5	4.25
12	48	1002	50	70	0.72	0.67	7.4	0.20	0.129	67.9	3.85
13	48	1002	50	70	0.70	0.65	10.3	0.28	0.123	64.7	3.79
14	48	1002	100	140	2.22	2.12	10.3	0.28	0.291	76.5	1.37
15	50	993	100	140	2.30	2.20	10.8	0.29	0.307	80.8	1.40
16	50	993	50	70	1.36	1.31	10.8	0.29	0.111	58.4	1.70
17	50	1007	101	142	1.00	0.90	(c)	(c)	0.380	99.0	4.18
18	50	1006	50	70	0.50	0.45	(c)	(c)	0.187	98.5	8.31
19	50	1006	100	140	2.28	2.18	16.8	0.45	0.331	87.2	1.52
20	50	1006	50	70	0.67	0.62	16.8	0.45	0.141	74.4	4.56
21	50	1008	150	210	2.81	2.66	16.8	0.45	0.506	88.9	1.27

(a) Electrode Area (8 through 10) = 0.75 cm^2; thickness = 2.0 mm
(b) Electrolysis of air
(c) Oxygen electrolysis; j'_{O_2} = 6.0 ml/min
(d) Electrode area (11 through 21) = 0.71 cm^2; thickness = 2.0 mm

Table 3-6(Cont.)

Run	Note-book page	t (° C)	i (mA)	i/A (mA/cm^2)	E (V)	E Corrected for IR in leads	j'_{CO_2} (ml/min)	j'_{H_2O} (ml/min)	j_{O_2} (ml/min)	C. E.$_{(O_2)}$ (%)	O_2 Yield $\frac{ml/min}{watt}$
22[h]	56	1000	50	70	0.46	0.30	(e)	(e)	0.188	99.0	12.50
23	56	1000	100	140	0.87	0.55	(e)	(e)	0.375	98.9	6.82
24	56	1000	150	210	1.27	0.79	(e)	(e)	0.551	96.9	4.65
25	56	987	50	70	0.52	0.36	(b)	(b)	0.186	98.0	10.33
26	56	986	100	140	0.91	0.59	(b)	(b)	0.386	101.0	6.55
27	58	984	50	70	1.87	1.71	(f)	(f)	0.115	60.6	1.34
28	58	983	50	70	1.77	1.61	(g)	(g)	0.118	62.2	1.47
29	58	983	100	140	2.38	2.06	(g)	(g)	0.275	72.5	1.34
30[i]	60	848	100	140	2.76	2.48	(b)	(b)	0.313	80.3	1.26
31	60	842	100	140	3.48	3.20	5.3	0.14	0.218	57.5	0.68
32	60	839	50	70	2.34	2.20	11.1	0.30	0.091	48.0	0.83
33	60	840	150	210	4.16	3.74	11.1	0.30	0.300	52.6	0.53
34	60	839	75	105	2.91	2.70	11.1	0.30	0.143	50.2	0.71

(b) Electrolysis of air
(c) Oxygen electrolysis; j'_{O_2} = 6.0 ml/min
(d) Electrode area (11 through 21) = 0.71 cm^2; thickness = 2.0 mm
(e) Oxygen electrolysis; j'_{O_2} = 1.0 ml/min
(f) Electrolysis of 25.9% CO + 74.1% CO_2; j'_{CO/CO_2} = 10 ml/min
(g) Electrolysis of 25.9% CO + 74.1% CO_2 with water vapor; j'_{CO/CO_2} = 13.4 ml/min j'_{H_2O} = 0.36 ml/min
(h) Electrode area (22 through 29) = 0.71 cm^2; thickness = 1.30 mm
(i) Electrode area (30 through 34) = 0.71 cm^2; thickness = 1.30 mm

Table 3-7

COMPARISON OF SIMILAR ELECTROLYSIS RUNS

$(ZrO_2)_{0.82}(CaO)_{0.15}(CeO_2)_{0.03}$

	Run	t (°C)	i/A (mA/cm^2)	C.E.$_{(O_2)}$ (%)	O_2 Yield $\frac{ml/min}{watt}$
CO_2-H_2O ELECTROLYSIS	10	986	67	82.6	3.65
	12	1002	70	67.9	3.85
	13	1002	70	64.7	3.79
	16	993	70	58.4	1.70
	20	1006	70	74.4	4.56
	14	1002	140	76.5	1.37
	15	993	140	80.8	1.40
	19	1006	140	87.2	1.52
AIR ELECTROLYSIS	8	986	68	100	4.95
	25	987	70	98.0	10.33
OXYGEN ELECTROLYSIS	18	1006	70	98.5	8.31
	22	1000	70	99.0	12.50
	11	1004	140	99.5	4.25
	17	1007	142	99.0	4.18
	23	1000	140	98.9	6.82

Plots of the cell voltage corrected for lead resistance against the current are given in Figs. 3-6 and 3-7 for the ceria-free electrolyte and for the 3 mole % ceria electrolyte respectively. The plots obey Eq. (3-13) with an activation polarization of the order of a few hundred millivolts or less, and a small contact resistance. In the runs with $CO_2 - H_2O$, the reversible voltage will be established by the steady state concentration of CO that builds up near the cathode as a reaction product. This value will be $\sim 1V$. Greater precision in interpreting electrolysis runs of this type can be attained by electrolysing a feed stream of a $CO - CO_2$ mixture at a flow rate and at currents such that the change produced in the $CO - CO_2$ ratio is negligible. Under these conditions, concentration polarization, E_c, will be absent and E_N will remain fixed at a known value that can be calculated from the equilibrium constant for the reaction

$$CO + \frac{1}{2} O_2 \rightleftarrows CO_2 \qquad (3\text{-}14)$$

and the Nernst equation, throughout the electrolysis run. It is anticipated that improvements in our experimental technique will enable the contact resistance to be reduced to a negligible value.* It will be possible in the future to obtain E_p accurately from the intercept and R_o from the slope of a E-I plot and thus to calculate the applied voltage for some standard electrolyte thickness (e.g., 1.0 mm). Using this calculated E_A, more meaningful oxygen energy yield values can be obtained, permitting better comparison of different electrolyte compositions.

A comparison of the two electrolyte compositions used in the runs performed to date is given in Table 3-8. It is evident that the loss in current efficiency resulting from the component of electronic conductivity in the 3 mole % ceria electrolyte has been compensated by the lower voltage required to sustain a given current density.

---

*Contact resistance has not been a problem previously as our results on conductivity measurements compared with literature and previously reported bears out. The problem with sealed disks has arisen because of experimentation with a different method in applying electrode contacts. By comparison with previous results on conductivity and taking disk electrolyte geometry into account we can determine if contact resistance has been minimized.

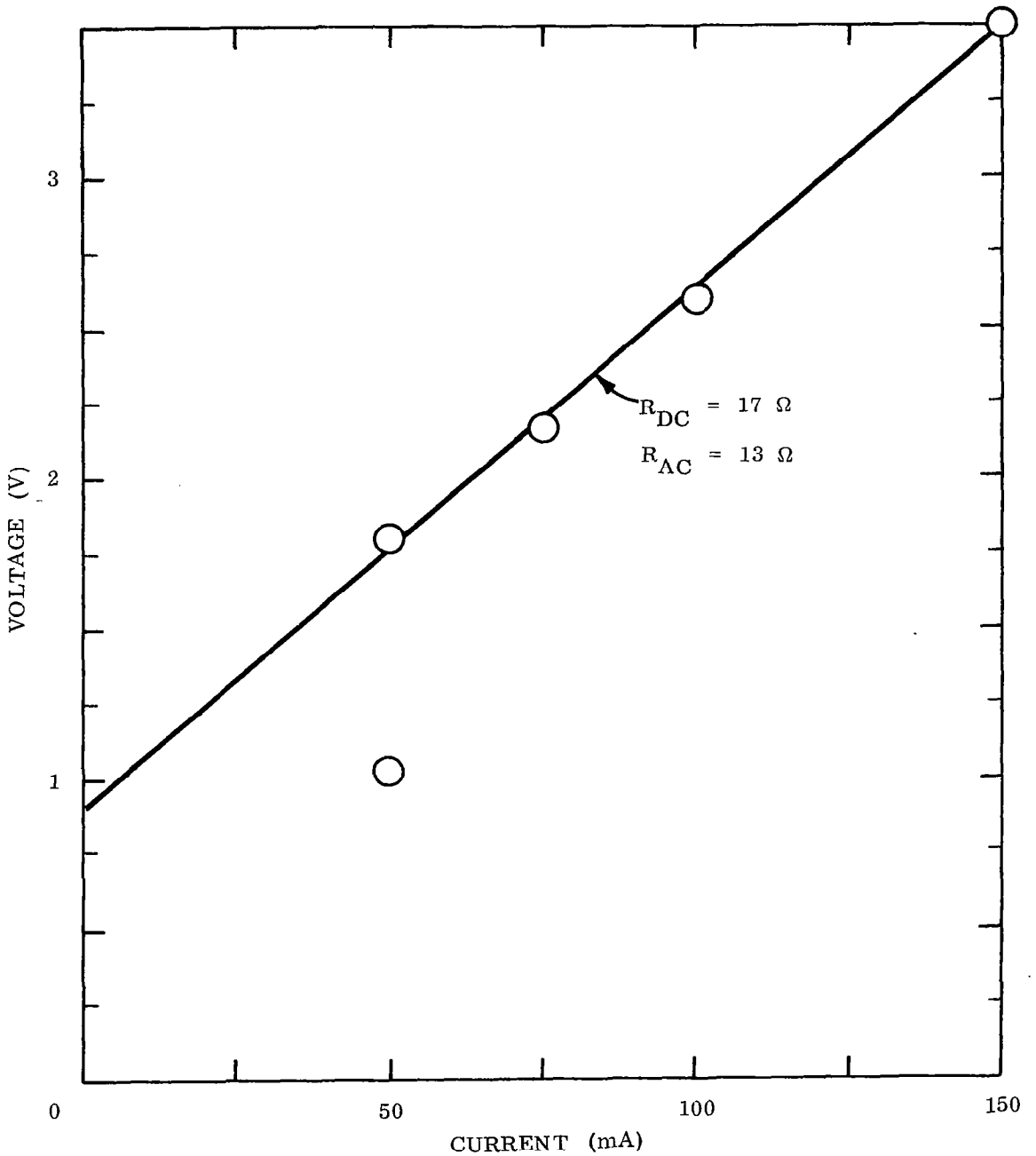

Fig. 3-6 E-I Plot for $(ZrO_2)_{0.85}(CaO)_{0.15}$ at 982 °C
Electrode Area = 0.71 cm^2
j'_{CO_2} = 8.8 ml/min; j'_{H_2O} = 0.22 ml/min

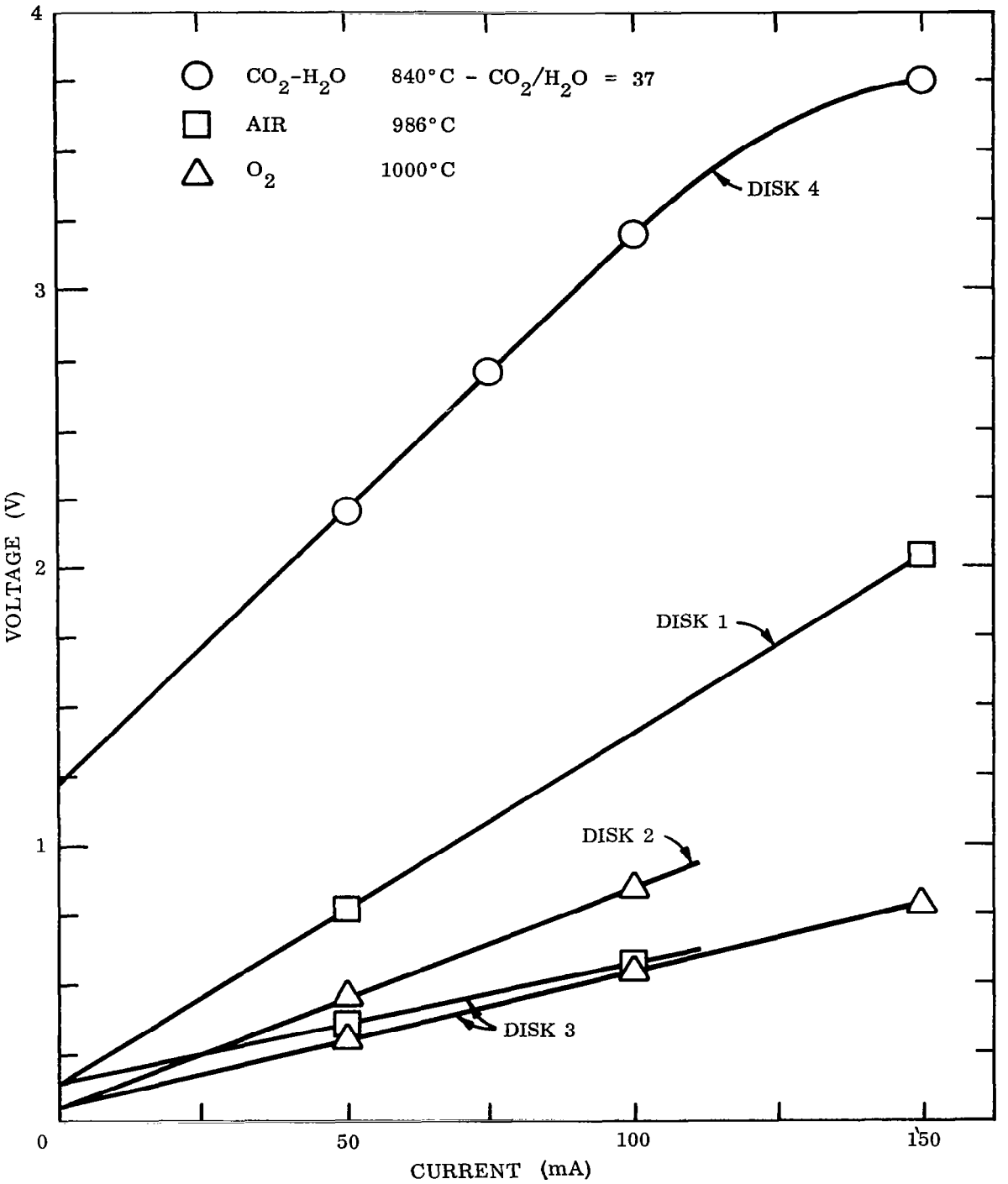

Fig. 3-7 E-I Plot for $(ZrO_2)_{0.82}(CaO)_{0.15}(CeO_2)_{0.03}$
Disk 1: Electrode Area = 0.75 cm^2
Disks 2,3,4: Electrode Area = 0.71 cm^2

The resultant oxygen energy yields are similar for the two compositions, within the limits of error of these experiments.

Table 3-8

COMPARISON OF PERFORMANCE OF CERIA-CONTAINING ELECTROLYTE WITH CERIA-FREE ELECTROLYTE

$(ZrO_2)_{0.85}(CaO)_{0.15}$						$(ZrO_2)_{0.82}(CaO)_{0.15}(CeO_2)_{0.03}$				
Run	t (° C)	i/A (mA/cm^2)	C.E.O_2 (%)	O_2 Yield (ml/min/W)		Run	t (° C)	i/A (mA/cm^2)	C.E.O_2 (%)	O_2 Yield (ml/min/W)
2	982	70	96.8	2.03	⟷	10	986	67	82.6	3.65
4	982	140	99.5	1.46	⟷	15	993	140	80.8	1.40
6	841	70	100.0	0.83	⟷	32	839	70	48.0	0.83
7	841	105	74.1	0.47	⟷	34	839	105	50.2	0.71
5	986	210	101.0	1.10	⟷	21	1008	210	88.9	1.27

Electrolysis experiments with 6.5, 10, and 15 mole % ceria disk cells do not give reproducible values for oxygen current efficiencies, and this behavior seems to be related to changes in the oxidation state of the electrolyte. When no current is flowing in the external circuit a difference in oxygen partial pressures on the two sides of the cell will cause oxygen to be transferred ionically through the electrolyte at a rate determined by the degree of electronic conductivity of the electrolyte. Since the electrolyte resistance rises rapidly as the temperature is lowered, the rate of ionic oxygen transport will fall off sharply at lower temperatures. The experimental observation that the rate of oxygen flow from the oxygen side of the cell into the CO-CO_2 side did not decrease as the temperature was lowered from 1000° to 300°C indicates that a transport mechanism other than ionic is involved in addition to ionic transport. It does not appear as if the seals are leaking as tested by pressuring one side of the cell and looking for gas flow from the other side and also by observing the correct EMF for the cell O_2/air. Furthermore, an oxygen flow of this type is not a problem when the electrolyte contains no ceria.

The effect of this flow of oxygen on the results of CO_2 electrolysis experiments is to decrease the current efficiency and also to interfere seriously with the reproducibility of the runs since the flow rate changes. It might be that the transport mechanism depends upon the oxidation state of the ceria in the electrolyte. As electrolysis proceeds, the CO/CO_2 ratio at the cathode increases and the concentration of Ce^{+3} ions on that side of the electrolyte disk will be correspondingly increased. Since the disk must be completely oxidized on the oxygen side, however, the manner in which the oxygen completes its penetration of the disk is difficult to envision. A further possibility is that the gold compression seals become leaky for some reason with ceria-containing disks that have been partially reduced.

One piece of evidence that rapid oxygen transport into the electrolyte can occur at a rate much greater than the ionic mechanism can sustain is provided by the re-oxidation rate of disks previously reduced in $CO-CO_2$ mixtures. An example is shown in Fig. 2-15. As the reduced disk is heated in oxygen, complete re-oxidation occurs within a few seconds at a temperature of 300°C or lower. This indicates that oxygen is penetrating into the interior of the samples, which are several millimeters in thickness, in several seconds. The current equivalent to oxygen ion transport is given by

$$i_{O_2} = \frac{A}{\ell} \sigma t_{o^=} t_{e^-} E \quad \text{(Ref. 35)} \qquad (3\text{-}15)$$

where

- A = electrolyte area
- ℓ = electrolyte thickness
- σ = conductivity
- $t_{o^=}$ = transport number of the oxide ions
- t_{e^-} = transport number of the electrons
- E = theoretical voltage

Using this relation, an approximate calculation can be made for the time required for ionic oxygen transport in the amount equal to that lost and gained during the reduction and oxidation runs of the microweighing experiments. Considering oxygen transport

through a 1 cm^2 cross section and an electrolyte thickness of 0.1 cm between oxygen partial pressures of 1 atm and 10^{-30} atm (i.e., equivalent to 25.9% CO in CO_2) at 500°C for the 15 mole % ceria electrolyte, the parameters are:

$A = 1\ cm^2$

$\ell = 0.1$ cm

$\sigma = 10^{-4}\ ohm^{-1}cm^{-1}$

$E = 1.15$ volts

$t_{o=} = t_{e-} = 1/2$ since this value maximizes the $t_{o=} t_{e-}$ product

The oxygen ion current is then 0.29 mA. The oxygen actually lost in the reduction experiments in 25.9% CO in CO_2 was 5.9 mg for a sample of 782 mg, and using this proportion, the oxygen lost for a 1 $cm^2 \times 0.1$ cm disk (density = 5.73 g/cm^3) would be 4.28 mg. At an ionic current of 0.29 mA, the time required to transfer 4.28 mg would be 45.3 hr. As Fig. 2-15 shows, the actual time required in the re-oxidation runs was of the order of seconds, not hours.

An example of the effect of the back flow is provided by two runs with a 6.5 mole % ceria disk cell in which 1.6% CO in CO_2 was electrolyzed at 859° with and without an air flow through the anode chamber. The back flow rate at zero current was 0.08 ml/min (equivalent to 21 mA). With an electrolysis current of 50 mA and no anode air flow, the oxygen current efficiency was 58% as determined from the gas flow out of the anode chamber during electrolysis. When air was flowed through the anode chamber at a constant rate with no current and then the electrolysis current of 50 mA was turned on, the increase in the anode gas outflow corresponded to 0.19 ml/min or 100% oxygen current efficiency. However, if the current efficiency were based on the net oxygen output of the cell, namely the oxygen outflow minus the gas inflow on the anode side, then a value of 0.11 ml/min or 58% would result, in apparent agreement with the first run. From these runs, it seems as though there were a constant oxygen back flow (or leak) through the electrolyte disk into the CO-CO_2 side of the cell. The passage of electrolysis current caused oxygen to be evolved at the anode, part of which was lost via the back flow. Electrolysis runs with 10 and 15 mole % ceria electrolytes and runs with other 6.5 mole % ceria cells have proven much more difficult to interpret since the results were inconsistent from run to run. One possible explanation is that

the back flow rate was varying, and, in fact, some measurements of this rate at open circuit shortly after turning off the electrolysis current indicate that the rate does not remain constant.

The origin of the back flow will have to be traced before a rational treatment of these data can be made.

Section 4
ONE-EIGHTH MAN LABORATORY MODEL CO_2 ELECTROLYZER

The total requirement of oxygen (from both CO_2 and H_2O) for a one-eighth man electrolysis unit would be approximately 16 amps of ionic current. A unit capable of electrolyzing one-eighth of the carbon dioxide exhaled by one man would have a capacity of approximately 12 amps of ionic current. The discussion below relates only to the electrolysis of CO_2 at 12 amps of ionic current. If an operating temperature of 800 °C were chosen in order to broaden the range of suitable materials of construction, the current efficiency would be less than 100 %. By the use of an electrolyte containing a controlled amount of electronic conductivity, it is believed that operation at a current efficiency of approximately 75 % could be achieved at 800 °C and a current density of 100 mA/cm^2. Thus, a total current of 16 amps would be required to maintain 12 amps of ionic current, requiring an electrolyte area of 160 cm^2 at 100 mA/cm^2.

Construction of the electrolysis unit as a battery of disk cells with gas spaces between them has the advantage of compactness, and, by judicious choice of the individual disk diameter and of the number of disks, allows a unit to be built with a low ratio of external area to volume. This feature is an advantage in controlling heat loss and maintaining a uniform temperature within the unit. Eight disks, each with an electrode area of 20 cm^2 (electrode diameter of 5.05 cm), provide the necessary 160 cm^2. An additional 0.5 cm is provided at the edge of each disk for a gas-tight ceramic seal, making the disk diameter 6.05 cm. Allowing 0.5 cm for the gas spaces, and using ceramic end pieces 0.5 cm thick would make the electrolysis unit 6.3 cm in height and 6.05 cm in diameter exclusive of gas manifolds and electrical leads.

A unit of this type is shown in Fig. 4-1. The figure shows four gas manifolds, two on the CO-CO_2 sides and two on the oxygen side, although the oxygen side requires only an outlet in operation. An inlet might be useful for purging the oxygen gas spaces, however.

In operation at 16 amps total current (12 amps ionic, 4 amps electronic), 91.2 ml/min of CO_2 would be consumed to produce 91.2 ml/min of CO and 45.6 ml/min of O_2, calculated at 1 atm and 25 °C. The CO_2 inflow rate would be greater than 91.2 ml/min

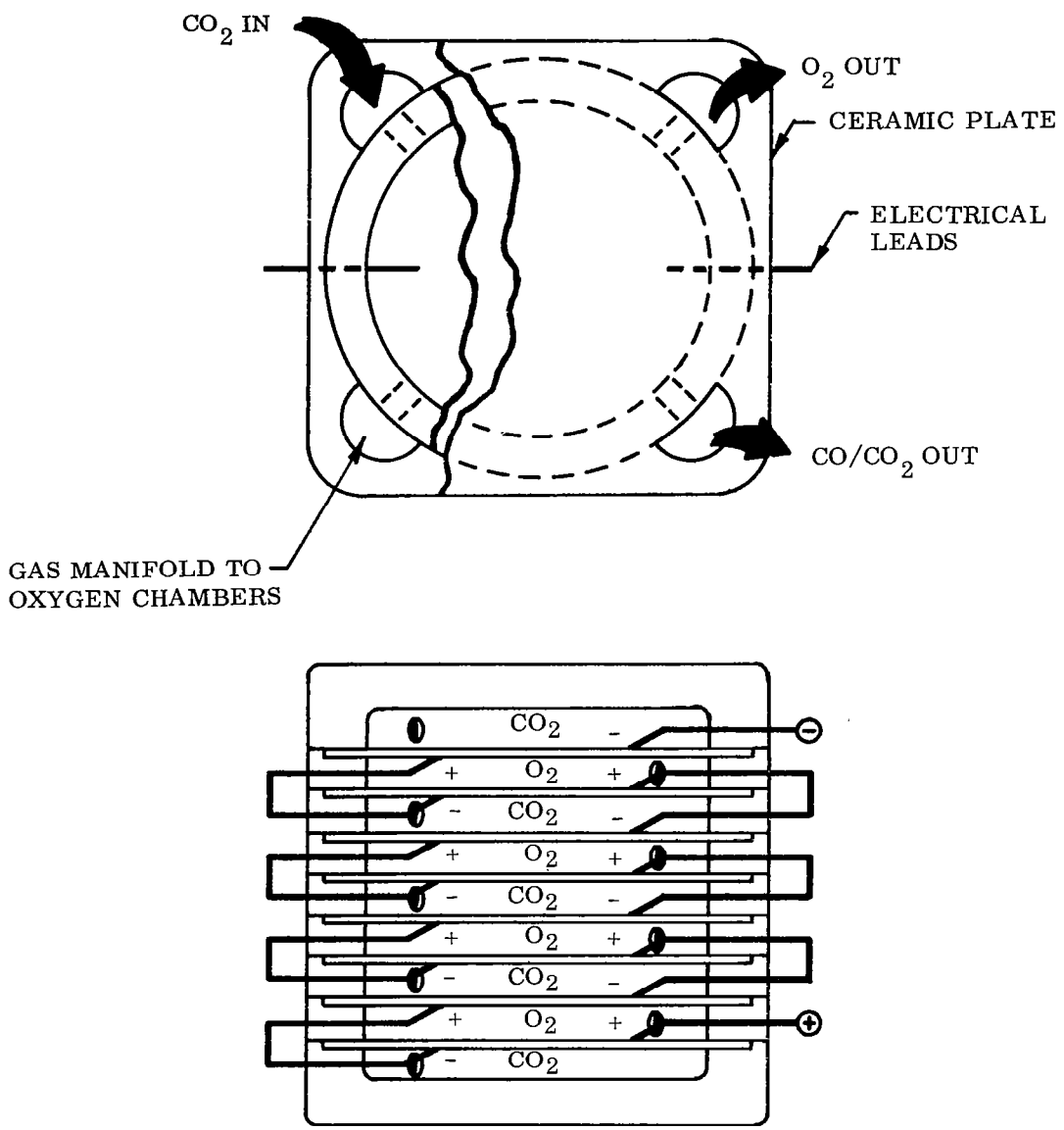

Fig. 4-1 One-Eighth Man Laboratory Model Carbon Dioxide Electrolyzer With External Series Connection

since 100% conversion could not be achieved on each pass through the cell for reasons of preventing concentration polarization and carbon deposition. At 800°C, carbon deposition is possible at CO concentrations greater than 90%. At a conversion rate of 50%, 182.4 ml/min of CO_2 containing a trace of water to catalyze the electrode reactions would enter the unit, 91.2 ml/min of CO and 91.2 ml/min of CO_2 would leave the cathode chambers and 45.6 ml/min of O_2 would leave the anode chambers (calculated at 1 atm, 25 °C). These rates correspond to 36.5 ml/min for each of the five cathode chambers and 11.4 ml/min for each of the four anode chambers (calculated at 1 atm, 25 °C.) At the operating temperature, 800 °C, these flow rates would be 131 ml/min and 41 ml/min respectively. With the dimensions of Fig. 4-1, the volume of each gas chamber is 10 ml.

Electrically, the disks are connected in series. Series connection is desirable to prevent breakdown that can occur with disks connected in parallel caused by a slight imbalance in the current heating one disk causing its resistance to fall because of the negative temperature coefficient of resistance of the electrolyte and therefore allowing more current to flow through that disk until a runaway condition develops in which most of the current flows through just one of the parallel-connected disks. This excessive current in one disk could result in failure of the unit by local overheating and cracking of the electrolyte. With series connection and control of the current, breakdown of this type can not occur. The individual cell voltage would be approximately 4 volts at the operating current of 2 amps. The unit, therefore, would require 32 volts and 2 amps or 64 watts for electrolysis.

An alternate method of constructing the stack of disks is shown in Fig. 4-2. The disks are sealed to metal segments containing a septum that divides the space between disks into two gas chambers. The electrodes are in electrical contact with the metal segments which serve to connect the disks in series electrically. This design has the advantage that electrical leads need be brought out only from the end cells, but it suffers the disadvantage of requiring a metal that can be used at 800°C in both oxidizing and reducing atmospheres and is thermally compatible with the ceramic electrolyte.

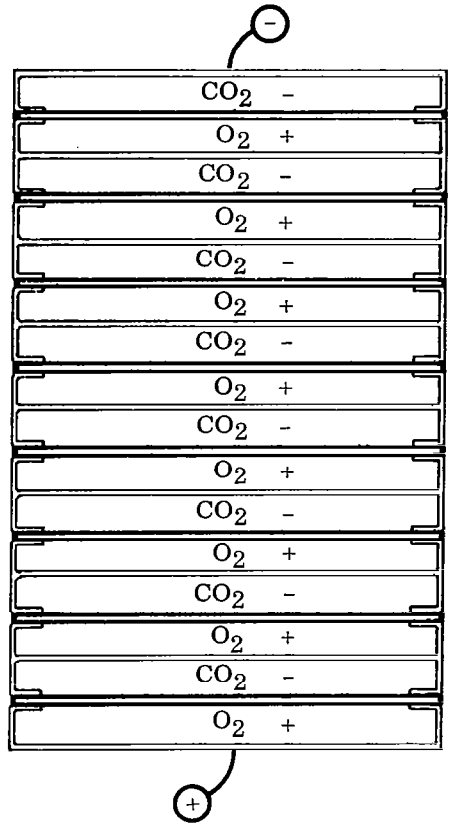

Fig. 4-2 One-Eighth Man Laboratory Model Carbon Dioxide Electrolyzer With Internal Series Connection

The actual construction of a working model similar to these designs would entail a great deal of experimentation to determine which techniques were most promising for making high temperature seals, gas manifolding, handling of the electrical leads and connections, and preventing thermal cracking in the electrolyte.

Section 5
REFERENCES

1. W. Nernst, Z. Elektrochem. 6, 41 (1900)
2. J. L. Weininger and P. D. Zemany, J. Chem. Phys., 22, 1469 (1954)
3. J. Weissbart and R. Ruka, Electrochemical Society Fall Meeting, Detroit, Michigan (2 – 5 Oct 1961), Extended Abstract No. 44, Battery Division
4. W. Schottky, Wiss. Veroff. Siemens-Werken 14, 1 (1935)
5. E. Baur and H. Preis, Z. Elektrochem., 43, 727 (1937)
6. G. H. J. Broers, Thesis, University of Amsterdam, The Netherlands (1958)
7. J. Weissbart and R. Ruka, J. Electrochem. Soc., 109, 723 (1962)
8. H. Binder, A. Kohling, H. Krupp, K. Richter and G. Sandstede, Electrochimica Acta, 8, 781 (1963)
9. A. D. Neuimin, S. V. Karpachev, and S. F. Pal'guev, Doklady Akademii Nauk SSSR, 141, 402 (1961) (English Translation)
10. J. Weissbart, LMSC, unpublished data
11. H. W. Chandler and W. Oser, Report No. MRL-TDR-62-16, Isomet Corporation, Palisades Park, New Jersey, Mar 1962
12. H. Chandler, Report No. AMRL-TDR-64-62, Isomet Corporation, Palisades Park, New Jersey, May 1964
13. H. H. Mobius, Z. fur Chem., 4, 81 (1964)
14. F. Hund, Z. Physik. Chem., 199, 142 (1952)
15. P. Duwez, F. Odell, and F. H. Brown, Jr., J. Am. Ceram. Soc., 35, 107 (1952)
16. F. Dietzel and H. Tober, Ber. deut. Keram. Ges., 30, 47, 71 (1953)

17. Z. S. Volchenkova and S. F. Palguev, Trans. Inst. Electrochem. No. 1, 97, Consultants Bureau, New York (1961)

18. T. Y. Tien and E. C. Subbarao, J. Chem. Phys., 39, 1041 (1963)

19. J. Weissbart and L. S. Rowley, Electrochem. Soc., Extended Abstracts, No. 31, Vol. 9, (Oct 1964)

20. F. Trombe and M. Foex, Compt. rend., 236, 1783 (1953)

21. H. A. Johansen and J. G. Cleary, J. Electrochem. Soc., 111, 100 (1964)

22. E. K. Keler, N. A. Godina, and A. M. Kalinina, J. Inorg. Chem. USSR, 1, 2556 (1956), Transl. J. Inorg. Chem. V, 127 (1956)

23. S. F. Palguev, S. V. Karpachev, A. D. Neuimin, and Z. S. Volchenkova, Doklady Akad. Nauk SSSR, 134, 1138 (1960)

24. P. Duwez and F. Odell, J. Am. Ceram. Soc., 33, 274 (1950)

25. K. Kiukkola and C. Wagner, J. Electrochem. Soc., 104, 379 (1957)

26. J. B. Nelson and D. P. Riley, Proc. Phys. Soc. (London) 57, 160 (1945)

27. A. Rabenau, Z. Anorg. Allgem. Chem., 288, 221 (1956)

28. W. R. Ruby and R. P. Loveland, J. Phys. Chem., 50, 345 (1946)

29. W. D. Kingery, J. Pappis, M. E. Doty, and D. C. Hill, J. Am. Ceram. Soc., 42, 393 (1959)

30. W. H. Rhodes and R. E. Carter, Presented at the Am. Ceram. Soc. Meeting, Apr 1962. Abstract in Bull. Am. Ceram. Soc., (Apr 1962)

31. J. Weissbart and R. Ruka, Rev. Sci. Instr., 32, 593 (1961)

32. G. Brauer and K. Gingerich, J. Inorg. Nucl. Chem., 16, 87 (1960)

33. G. Brauer, K. Gingerich, and U. Holtschmidt, J. Inorg. Nucl. Chem., 16, 77 (1960)

34. L. S. Darken and R. W. Gurry, J. Am. Chem. Soc., 67, 1401 (1945)

35. C. Wagner, Z. Physik Chem. (Leipzig), B21, 25 (1933)

36. J. P. Coughlin, "Heats and Free Energies of Formation of Inorganic Oxides," U.S. Bureau of Mines, Bull. 542 (1954)